

24 GHz Flexible Antenna for Doppler Radar based Human Vital Signs Monitoring

Nitin Kathuria

A thesis submitted to

Auckland University of Technology

in partial fulfilment of the requirements for the degree of

Master of Engineering (ME)

2020

School of Engineering, Computer and Mathematical Sciences

Acknowledgements

Firstly, I would like to acknowledge and extend my heartfelt gratitude to my supervisor Dr. Boon-Chong Seet for his supervision, advice, and guidance from the very early stage of this research as well as for giving me extraordinary experiences throughout the work. Above all and the most needed, he provided me unflinching encouragement and support in various ways. I could never have embarked upon and started all of this without his prior teachings which opened up unknown areas to me.

I would like to thank Dr. Jack Xuejun Li for his advice and guidance during the initial phase of this research. I am grateful in every possible way and hope to continue our collaboration in the future.

Many thanks go, in particular, to PhD students Brandt Li, Aayush Aneja and Adnan Ghaffar, for their timely support, guidance, and for providing technical expertise, and valuable advice in helping to resolve some critical issues of this research.

I would also like to thank the Jian Huang, Senior Electronics Technician for his excellent support and suggestions throughout my research work.

I wish to express my love and gratitude to my beloved Father Late Sri N. K Kathuria who left us for heavenly abode during studies. His blessings are needed always. And my biggest thanks to my mother Smt. Usha Kathuria and my sister Neha Kathuria Bhatnagar and Brother-in-law Piyush Bhatnagar for all the support you have shown me through this research. I would also like to thank my friends Aditya Sahi and Karan Mhapankar for their contribution in taking out time for testing.

Special thanks to my wife Jyoti Kathuria who has been extremely supportive of me throughout this entire process and has made countless sacrifices to help me get to this point and son Arjun who provided motivation to finish my degree with expediency, regardless of the distance apart.

Abstract

Noncontact monitoring of human vital signs is an emerging research topic in recent years. A key approach to this monitoring is the use of the Doppler radar concept which enables real-time vital signs detection, resulting in a new class of radar system known as bio-radar. Unlike traditional techniques that use contact electrodes for vital sign measurement, bio-radar is non-intrusive and less perturbing for infants and patients with critical injuries. The bio-radar can even detect life under rubble in the aftermath of disasters. The antennas are a key component of any bio-radar module and their designs should meet the common requirements of bio-radar applications such as high directivity, circularly polarized, and flexibility.

This thesis presents the design of a 24 GHz four-element antenna array on a low-cost and flexible liquid crystal polymer (LCP) substrate with a thickness of only 100 μm , low-loss tangent ($\tan\delta=0.0021$), stable dielectric constant ($\epsilon_r=3.35$) and low moisture permeability. The designed antenna array can be used with a bio-radar for vital signs monitoring in a non-contact manner. To the best of our knowledge, the design of flexible antenna arrays for bio-radar and the use of LCP for such applications have not been explored in literature.

Any antenna array will require a unit element to be designed first. The unit element was designed with an input impedance of 50 Ω on LCP substrate, which is then used to construct a two- and four-element array with an overall dimension of 29.5 \times 25.4 mm, and 53 \times 36.5 mm, respectively. The simulated gain obtained is 4.39 dB, 5.46 dB, and 6.68 dB for unit cell, two-element array, and four-element array, respectively. Other measured and simulation results showed close agreement. The two vital signs: breathing rate (BR) and heart rate (HR) of two human subjects are detected with relatively good accuracy using the fabricated antenna arrays and RF output power of -3 dBm from a distance of approximately 60 cm.

Table of Contents

Acknowledgements	i
Abstract.....	ii
Table of Contents.....	iii
List of Figures	v
List of Tables	vi
Chapter 1: Introduction	1
1.1 Motivation and Scope	2
1.2 Contributions.....	2
1.3 Thesis Organisation	3
Chapter 2: Background and Literature Review	4
2.1 Antenna Principles	4
2.1.1 Radiation Pattern.....	4
2.1.2 Near & Far-Field Regions.....	5
2.1.3 Directivity and Gain.....	6
2.1.4 Polarization and Axial Ratio	7
2.1.5 Antenna Bandwidth (BW)	8
2.1.1 Voltage Standing Wave Ratio (VSWR) and Return Loss.....	8
2.2 Microstrip Patch Antenna	9
2.3 Array Antenna.....	10
2.3.1 Linear Array Factor.....	11
2.3.2 Planar Array Factor	12
2.4 Bio Radar Theory	13
2.4.1 CW Radar.....	14
2.4.2 FMCW Radar.....	14
2.4.3 UWB Radar.....	14
2.5 HR and BR Measurement	15
2.5.1 Chest movement.....	15
2.5.2 Respiratory rhythm	17
2.6 Doppler Radar.....	17
2.7 Literature Review.....	19
2.7.1 Directivity	19
2.7.2 Frequency.....	19
2.7.3 Compactness	20

2.7.4 Polarization	20
2.7.5 Flexibility	21
2.8 Summary	21
Chapter 3: Research Methodology	22
3.1 Antenna Design and Simulation	22
3.2 Antenna Fabrication.....	22
3.2.1 Laser Cutting.....	22
3.2.2 Photoetching	22
3.3 Antenna Characterization.....	23
3.4 HR and BR Signal Acquisition	23
3.5 HR and BR Signal Processing	24
3.5.1 Fast Fourier Transform	25
3.5.2 Filtering.....	25
3.5.3 Smoothing	26
3.5.4 Peak Detection	26
3.6 Summary	26
Chapter 4: Proposed Antenna Designs	27
4.1 Single-element unit cell	27
4.2 Two-element array	28
4.3 Four-element array	28
4.4 Summary	30
Chapter 5: Results and Discussion	31
5.1 Simulated Antenna Performance	31
5.2 Measured Antenna Performance.....	37
5.3 Measured Bending Analysis	41
5.4 Measured Heart Rate and Breathing Rate.....	42
Chapter 6: Conclusion and Future Work.....	46
References	47

List of Figures

Figure 1: Representation of Radiation Pattern (Balanis 2016)	5
Figure 2: Coordinate arrangement (Balanis 2016).....	5
Figure 3: Polarisation ellipse (Balanis 2016).....	8
Figure 4: Microstrip Patch Antenna (Balanis 2016)	9
Figure 5: Planar array representation (Balanis 2016)	12
Figure 6: Radar types	13
Figure 7: Modes of Operation of RADAR for Vital Sign Measurement	14
Figure 8: Heart anatomy and episodes of heart beat (Boric-Lubecke 2015, Park et al. 2019)	16
Figure 9: ECG output.....	17
Figure 10: Doppler Effect	18
Figure 11: Setup for HR and BR measurement	24
Figure 12: Signal processing steps to determine HR and BR	24
Figure 13: Magnitude response of a typical filter	26
Figure 14: Single-element unit cell.....	27
Figure 15: Two-element array	28
Figure 16: Four-element array	29
Figure 17: Fabricated antenna samples	29
Figure 18: Single element return loss $ S_{11} $	31
Figure 19: Two-element array return loss $ S_{11} $	32
Figure 20: Four-element array return loss $ S_{11} $	32
Figure 21: Radiation pattern of (a) single-element unit cell; (b) two-element array; (c) four-element array. The plot for $\varphi=0^0$ and $\varphi=90^0$ refers to the E-plane (side-view) and H-plane (top-view), respectively	33
Figure 22: 3D polar plot for (a) single-element unit cell; (b) two-element array; (c) four-element array	34
Figure 23: Gain versus Theta (θ) for (a) single-element unit cell; (b) two-element array; (c) four-element array, with $\varphi=0^\circ$ (red) and $\varphi=90^\circ$ (purple).....	35
Figure 24: Axial ratio vs Theta (θ) for (a) single-element unit cell; (b) two-element array; (c) four-element array.....	37
Figure 25: Example return loss measurement of a unit cell using the VNA.....	37
Figure 26: Measured return loss of (a) unit cell; (b) two-element array; (c) four-element array.....	38
Figure 27: Example S_{21} measurement of a unit cell using the VNA.....	39
Figure 28: Measured gain of (a) unit cell; (b) two-element array; and (c) four-element array.....	40
Figure 29: Example measurement setup for bending analysis.....	41
Figure 30: Comparative bending analysis of return loss S_{11}	42
Figure 31: (a) Example setup for HR/BR measurement; (b) Subject sitting in front of the setup	43
Figure 32: Example measurement of true HR of: (a) Subject 1 (male); and (b) Subject 2 (female); using a wrist-worn HR monitor	43
Figure 33: One HR/BR measurement of Subject 1 using two-element array (HR: 94, BR:18)	44
Figure 34: One HR/BR measurement of Subject 1 using four-element array (HR: 91, BR:14).....	45
Figure 35: One HR/BR measurement of Subject 2 using two-element array (HR: 73, BR:17)	45
Figure 36: One HR/BR measurement of Subject 2 using four-element array (HR: 82, BR:12).....	45

List of Tables

Table 1: Common suitable substrates available for antenna (Balanis 2016).....	16
Table 2: Estimated and True HR and BR from two human subjects.....	41

Attestation of Authorship

“I hereby declare that this submission is my own work and that, to the best of my knowledge and belief, it contains no material previously published or written by another person (except where explicitly defined in the acknowledgements), nor material which to a substantial extent has been submitted for the award of any other degree or diploma of a university or other institution of higher learning.”

Signed:

Date: 04 February 2021
.....

Chapter 1: Introduction

In today's hectic pace of life, there is an increasing risk of lifestyle disorders such as cardiovascular diseases, hypertension and diabetes. Hence, the measurement of physiological signals for timely detection of such disorders is increasingly important in the healthcare sector. The vital signs of interest frequently include the heart rate (HR) and breathing rate (BR).

Radar-based vital signs monitoring is a new technology that leads to the concept of *bio-radar* (Gouveia, Malafaia et al. 2018), which together with other flexible and wireless physiological sensors, promise to revolutionize the healthcare industry. It may be also used to detect life in search and rescue operations after disasters (Mpanda, Liang et al. 2018).

Radar is a technology that detects radio signals from a target device and measures its positional value and velocity in a three-dimensional plane. It was initially developed for military applications to locate enemy planes, but is presently being used for numerous civilian applications such as air traffic control, self-driving autonomous cars, radio astronomy, etc.

The concept of bio-radar uses Doppler radar to capture BR and HR information in a contactless way. In a typical continuous wave radar that operates on continuous wave signals, two antennas are used: one for the transmitter and another for the receiver. The transmitting antenna focuses the signal to the chest of the subject and the receiving antenna acquires the reflected signal, whose frequency changes due to micro-movements of subject's chest caused by breathing and heartbeat. This is known as the Doppler effect in which the received frequency increases or decreases as the target moves towards, or away from the radar, respectively (Boric-Lubecke, Park et al. 2015).

One cycle of a heartbeat involves contracting and pumping blood through the circulation system between the heart and the rest of the body (Ramachandran, Swarnamani et al. 1991). On the other hand, the respiration is a two-step quasi periodic activity which involves inhalation and exhalation (Tan and Hoole 1998). The HR and BR information embedded in the received radar signal can be extracted using appropriate digital signal processing algorithm.

The antennas are a key component of any bio-radar module as transmission and reception of the signal with minimum losses is the key to a successful operation. They can compose of a single element or an array of multiple elements, can be designed for different frequencies, and use different types of substrates. However,

their designs should meet the application requirements of the bio-radar, which include high directivity, circular polarization, flexibility, among others.

1.1 Motivation and Scope

Most conventional devices used for measuring the vital signs are in contact with the subject, which requires the sensing probes to be physically attach to the patient and the instrument, which limits the movements of the patient. Therefore, there is a need to research a better solution with similar accuracy as conventional devices.

The wearable sensors offer greater freedom of movements to the patients, but they are still invasive as they need to be in contact with the subject and may not be always comfortable to wear. The above reasons motivated our investigation into contactless-based sensing and the concept of bio-radar for human vital signs monitoring appears promising, as it can be used not only as a remote equivalent of conventional and wearable sensors for in-home patients, but also for detecting signs of life in search and rescue operations after disasters.

However, to the best of our knowledge, no flexible bio-radar system has been proposed in literature. The flexibility of the antennas, which act as sensors in the bio-radar system, can enable them to be deployed on a wider range of surfaces due to their inherent conformity. In turn, this can enable the system to achieve a measurement accuracy closer to that of conventional devices.

The scope of this project consists of two parts (software and hardware) with a focus on developing a compact, low-cost, flexible, and high-gain antenna for bio-radar. The software part includes the design and simulation of the antenna and digital processing of radar signals for the extraction of BR and HR information. The hardware part includes the fabrication and measurement of designed antenna, and signal acquisition from human subjects using the antenna and related equipment.

1.2 Contributions

This project makes the following contributions:

- Designed an eclipse-shaped patch antenna element (a.k.a. unit cell) on a flexible liquid crystal polymer (LCP) substrate for a 24 GHz bio-radar system.
- Designed a 2- and 4-element array using the same unit cell to achieve better directivity and circular polarization performance for the bio-radar application.
- Recommended the most suitable substrate material for the designed antennas upon a study on the type of flexible materials used in previous works.
- Recommended the most appropriate fabrication method for the designed antennas upon an experimentation with different fabrication techniques.

- Developed a MATLAB program to process the radar signals acquired by the antennas and extract the BR and HR information.

A conference paper based on this work has been accepted for oral presentation:

N. Kathuria and B.-C. Seet, “*24 GHz Flexible LCP Antenna Array for Radar-based Noncontact Vital Sign Monitoring*”, 12th Asia-Pacific Signal and Information Processing Association (APSIPA) Annual Summit and Conference, Auckland, New Zealand, December 2020.

1.3 Thesis Organisation

The remaining chapters of this thesis are organized as follows.

Chapter 2 firstly presents the background concepts and theories relevant to this research, including those on bio radar, heart rate (HR) and breathing rate (BR) measurement, Doppler radar, antenna principles, microstrip patch antenna and antenna array. Next, it reviews the existing literature on antenna designs for radar applications. The review is categorized by the radar’s antenna requirements, namely directivity, frequency, compactness, circular polarization, and flexibility.

Chapter 3 describes the methodology employed in this research, such as the software used for antenna design and simulation, methods of antenna fabrication and characterization, and methods of HR and BR signal acquisition and processing.

Chapter 4 presents three proposed antenna designs based on microstrip patch structure, including a single-element unit cell, two- and four-element array, for radar-based detection of HR and BR.

Chapter 5 discusses the simulated and measured performance of the designed antennas, as well as the accuracy of the measured HR and BR acquired by the antennas from two human subjects.

Chapter 6 concludes the thesis and suggests some directions for future work.

Chapter 2: Background and Literature Review

2.1 Antenna Principles

An accelerating or retarding charge creates a disturbance in space that spreads as a time varying electric and magnetic field, collectively called an electromagnetic wave (Balanis 2016). Such charge can be accelerated or retarded on a wire, which will then be called a wired antenna. Such wired antennas can be properly shaped to improve the radiation characteristics. For instance, single wire can be shaped as dipole antenna, twisted wire as helical antenna, and a set of wires as log periodic antenna. An accelerating or retarding current that is time varying in any metal will produce a radiation.

$$L \frac{dl}{dt} = Lq \frac{dv}{dt} = L * q * a \quad (1)$$

where L is the length of wire, q is the charge and a is the acceleration. In a broad sense, if a set of individually radiating wires are shaped and arranged properly, they will constructively interfere in the area of interest, thereby increasing radiation efficiency in the desired direction. However, in other directions, the energy is substantially reduced, which can be explained by the law of conservation of energy. For this reason, isotropic antennas do not exist in reality but they are still used mathematically for comparison purposes to all other antennas.

There are various fundamental parameters that can be considered when studying any antenna. The gravity of such parameters depends on the nature of antenna being designed. Some of the basic and commonly used properties are briefly discussed below.

2.1.1 Radiation Pattern

A mathematical function of a graphical representation of the radiation properties of the antenna as a function of space coordinates is called as radiation pattern (Balanis 2016). It is a graphical representation of points of electric or magnetic fields on a three-dimensional plot at a fixed radius. The amplitudes of power are normalized to a decibel scale so that the low power and high-power components of the signal can be contrasted together in a single graph.

The graph that represents radiation pattern can also be used to identify major lobes and minor lobes. The minor lobe includes the back and side. The major lobe is the portion that carries a significant amount of energy. It gives the sense of where the bore sight is (the axis along which the most useful amount of power is directed). The graph also illustrates several frequently used parameters, such as half power beam width (HPBW) and first null.

An antenna used in Wi-Fi-routers might want a large HPBW so that it can cover an entire floor and minimize the complexity of having multiple antennas. Likewise, some antennas like the ones used in satellites might require a highly focused beam (narrow HPBW) so that the information carrying wave can penetrate longer distances with less loss.

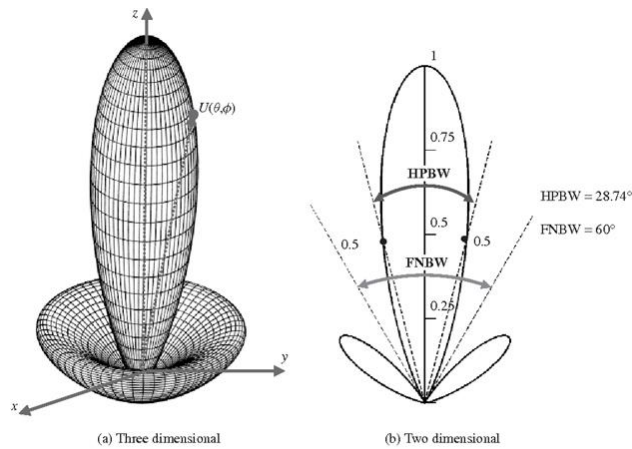


Figure 1: Representation of Radiation Pattern (Balanis 2016)

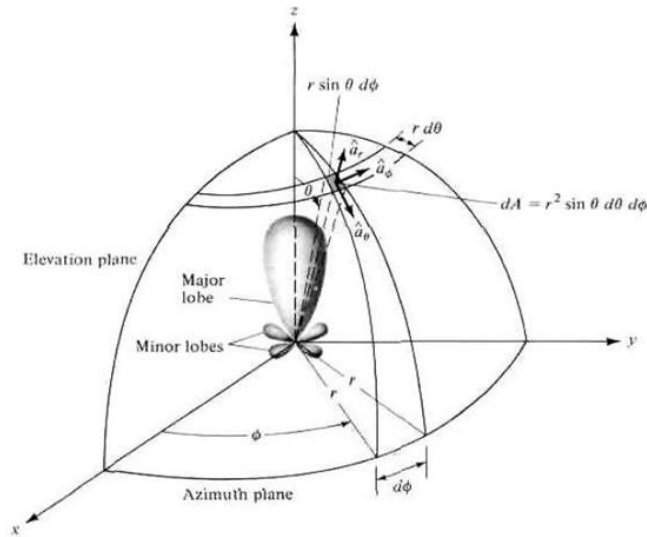


Figure 2: Coordinate arrangement (Balanis 2016)

2.1.2 Near & Far-Field Regions

To study the sensitive areas near an antenna, the area around it is generally classified into three regions. Though the regions are described by separate equations, it should be kept in mind that the region-classification may not always be realistic for all antennas, and further analysis may be required. Generally, the area in the vicinity of the antenna are distinguished as *Far Field* and *Near Field*. Near fields can further be discriminated as reactive and radiating fields. These fields depend on the point of observation from the antenna. The point of observation

or distance R depend on wavelength λ of signal and biggest dimension D of antenna. Equations (12), (13), and (14) defines R for the regions of reactive near field, radiating near field (Fresnel zone), and far field (Fraunhofer region), respectively.

$$R < 0.62 \frac{D^3}{\lambda} \quad (2)$$

$$0.62 \frac{D^3}{\lambda} < R < 2 \frac{D^2}{\lambda} \quad (3)$$

$$R > 2 \frac{D^2}{\lambda} \quad (4)$$

In far field region, the magnitude for electric and magnetic field follow the inverse square law. In far-field, the wave pattern is considered uniform, i.e. the wave can be considered to have a planar wave front. This the region where EM waves follow Maxwell's principles and both electric (E) and magnetic (M) waves are generated through each other. These E and H field vectors are 90° apart from one another and the direction of propagation is given by the cross product of the two vectors (Iskander 1992).

Near-field can be considered as a multipole whose field decay follows a combination of inverse square and inverse cubical law. Thus, such a field vanishes within a few λ away. In near field, EM waves are independent of each other. Some antennas can reliably operate using near-field radiation only. The near-field is also used in capacitive-sensing techniques. Such techniques are used to study the impact of objects like the human body in vicinity of the antenna. For example, smart watches have near field antennas and is always accompanied by a human wrist. Thus, the capacitive nature of the human body is considered when designing antennas for such a watch.

2.1.3 Directivity and Gain

Directivity can also be expressed as the ratio of radiation intensity (RI) of the antenna with that of an isotropic antenna:

$$D = \frac{U}{U_0} = \frac{4\pi U}{P_{rad}} \quad (5)$$

where U_0 is RI of a reference or isotropic antenna, and P_{rad} is net radiated power in watts. As radiation pattern of an isotropic antenna is a sphere, the directivity is one of a pattern uniformly distributed over a solid angle of 4π . The isotropic radiator is not practically available, as it is a pure theoretical concept. The most commonly available practical antenna that can be used as a reference is a dipole antenna, which has a directivity of 1.5.

Directivity also defines the direction of radiated or received power from/to the antenna as shown in (16) where P is power density at its maximum point and P_{avg} is average power density. Directivity helps in defining the functionality of the antenna. The antennas can be unidirectional, bidirectional or multi directional depending

upon the application. For an example, Yagi antenna is a directional antenna, while the antenna of a mobile device is often omnidirectional as the direction of the transmission is not fixed in a dynamic system.

$$D = \frac{P}{P_{avg}} \quad (6)$$

Because directivity is solely based on the shape of the radiative pattern of the antenna and it does not account for the losses that may actually occur in a real antenna system, a term called gain (G) is introduced (Balanis 2016), which is given by:

$$G = kD = \frac{P}{P_{avg}} \quad (7)$$

where, k is efficiency (i.e. power radiated divided by power input) of the antenna. Thus, for most of antennas whose efficiency is very high, gain is almost equal to directivity (Skolnik 2008). Generally, the sharper the lobe, the higher gain of the antenna will be (Mpanda, Liang et al. 2018). The overall gain for an antenna also depends on the transmission line that connects the power source. Such a transmission line has a different characteristic impedance than the antenna in general, which results in reflection of some signal. Such reflection generates reflection loss (also known as mismatch loss).

Gain is a unitless quantity and expressed in decibels (dBi or dBd) depending whether the reference antenna is an isotropic or dipole. (Balanis 2016). Gain in decibels $G(\text{dBi})$ of an antenna with respect to an isotropic antenna ($G_o = 1$) can be found by:

$$G(\text{dBi}) = 10 \log\left(\frac{G}{G_o}\right) \quad (8)$$

2.1.4 Polarization and Axial Ratio

Antenna generates an EM wave, in which there are three components: electric (E) field, magnetic (M) field, and direction of wave propagation. The polarization of an antenna refers to the direction of electric field of the generated EM wave. For a communication system, both transmitter and receiver should be similarly polarized for maximum power transfer, otherwise the polarization mismatch can cause significant power loss.

In EM wave, the E and H fields are perpendicular to each other. The H field surrounds the wire and perpendicular to it, which means the E field is parallel to the wire. The EM waves propagating in the same direction are called linearly polarized waves, and the direction can be either vertical or horizontal depending upon the antenna configuration. The direction of E field determined the polarization of the antenna. Other than linear polarization, there are also circular or elliptical polarization. The circular polarization can be right-handed or left-handed. The instantaneous E field propagating in the Z direction can be described by two orthogonal components as (Balanis 2016):

$$E_x(z, t) = E_{x0} \cos(\omega t + \beta z + \theta_x) \quad (9)$$

$$E_y(z, t) = E_{y0} \cos(\omega t + \beta z + \theta_y) \quad (10)$$

where E_{x0} and E_{y0} is the maximum amplitude of E fields in X direction, and Y direction, respectively, ω is the angular frequency, and β is the propagation constant.

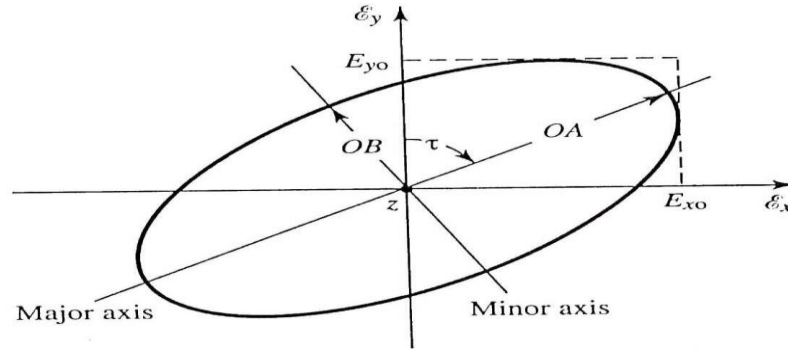


Figure 3: Polarisation ellipse (Balanis 2016)

The axial ratio of the polarization is defined as the ratio of major axis to minor axis of ellipse:

$$AR = \frac{E_x(z,t)}{E_y(z,t)} \quad (11)$$

If $AR = 1$, then both axes have the same amplitude, which represents circular polarization. On the other hand, if $AR = 0$ or ∞ , then it is linear polarization (Balanis 2016).

2.1.5 Antenna Bandwidth (BW)

The frequency range over which an antenna can show a specified level of performance is called the bandwidth of the antenna. The unit of measurement is in Hertz or a percentage of the antenna's design frequency.

Numerically:

$$BW = f_{max} - f_{min} \quad (12)$$

where f_{max} and f_{min} are the maximum and minimum frequency at which the antenna can show a specified level of performance. The percentage bandwidth of any antenna decreases if the frequency of operation is reduced. Therefore, for antennas operating at lower frequency, optimizing such antennas to achieve a larger bandwidth is a big challenge (Balanis 2016).

2.1.1 Voltage Standing Wave Ratio (VSWR) and Return Loss

Characteristic impedance mismatch can lead to large voltage standing wave ratio (VSWR) and return loss at the terminal. Both these parameters are dependent on the reflection coefficient (τ), which is defined as:

$$\tau = \frac{V^-}{V^+} = \frac{Z_L - Z_0}{Z_L + Z_0} \quad (13)$$

where V_0^- and V_0^+ is the reflected and incident voltage level respectively. The VSWR and return loss can be determined as a function of τ as:

$$VSWR = \frac{1+|\tau|}{1-|\tau|} \quad (14)$$

$$Return Loss(dB) = -20 \log_{10}(\tau) \quad (15)$$

In literature, the acceptable mismatch is 10% of the incident signal. Furthermore, as a rule of thumb in antenna design, the VSWR should be $1 < VSWR < 2$, and $Return Loss < -10 \text{ dB}$ (Balanis 2016).

2.2 Microstrip Patch Antenna

The growth in printed circuit board (PCB) technology has enabled printed antennas such as microstrip patch antenna. Despite having some disadvantages such as poor bandwidth and poor polarization purity, the convenience such antennas provide in terms of size, ease of fabrication, flexibility (in terms of several antenna parameters) and manufacturing cost are so attractive that copious amounts of research and investigations have been carried out on the patch antenna to improve and enhance its characteristics. In particular, with the emerging paradigm of Internet of Things (IoT) where all electronic devices are gradually being interconnected via wireless communication, this is also a perfect time to research on antennas that can have promising features in terms of power consumption, size and manufacturing cost.

In general, a microstrip patch antenna consists of three major parts: metallic patch, dielectric and ground plane. The space between the patch and ground is generally using a substrate with dielectric constant between 2.2 and 12. (Balanis 2016). A microstrip patch antenna using a thick substrate has low permittivity but large bandwidth and good efficiency. On the other hand, a thin substrate has higher dielectric constant that minimizes radiation. The dielectric constant or permittivity of a substrate affects the wavelength of the electromagnetic wave in that substrate. Since the patch length is directly influenced by wavelength, choosing the right substrate is very important, as it decides the size of the antenna. Patch antennas in general can be classified in terms of the shape of the patch. It can be rectangular, square, circular, elliptical, triangular, ring, or other shapes. Some commercially available substrates for patch antennae, along with key specifications, are shown in Table 1.

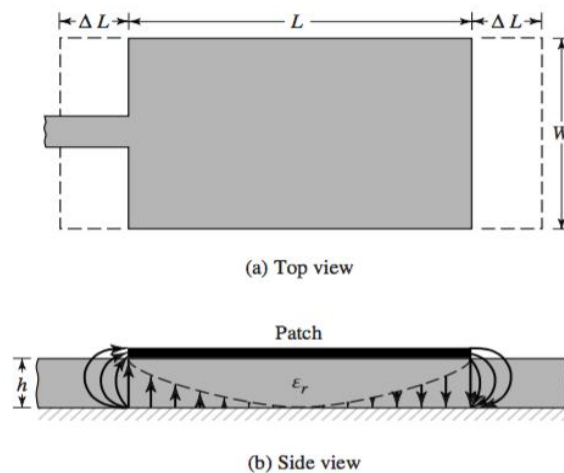


Figure 4: Microstrip Patch Antenna (Balanis 2016)

Table 1: Common suitable substrates available for antenna (Balanis 2016)

Manufacturer	Substrate	Thickness (mm)	Frequency (GHz)	ϵ_r	$\tan\delta$
Rogers	Duroid 5880	0.127	0 - 40	2.2	0.0009
	RO 3003	1.575	0 - 40	3.00	0.0010
	RO 3010	3.175	0 - 10	10.2	0.0022
	RO 4350	0.168 0.508 0.1524	0 - 10	3.48	0.0037
	FR4	0.05-100	.001	4.70	
DuPont	HK04J	0.025	0.001	3.50	0.005
Isola	IS 410	0.05—3.2	0.1	5.40	0.035
Arlon	Di Clad 870	0.091	0-10	2.33	0.0013
Polyflon	Polyguide	0.102	0-10	2.32	0.0005
Neltec	NH 9320	3.175	0-10	3.20	0.0024
Taconic	RF—60A	0.102	0-10	6.15	0.0038
Bakelite		1.5		4.78	0.03045
Duroid LCP	ULTRALAM 3908	50 um		2.9	0.004
Panasonic LCP	LCP(R-F705S)	100um	0-100	3.35	0.0021-0.0029

Patch antenna can be excited in different ways: using coaxial feed, strip line, microstrip line feed, proximity, and aperture coupling. The aperture and proximity coupling techniques of feeding the antenna can significantly increase the bandwidth but their fabrication process tend to be more difficult compared to the coaxial and microstrip feeding techniques.

Coaxial feeding uses the SMA or a coaxial connector to feed the patch. Here, the inner conductor of the cable is connected to the patch through microstrip-feeding technique, where a microstrip line of proper width serves as a transmission line for the patch from source. Generally, the transmission line penetrates the patch towards the area where the patch has impedance of nearly 50Ω for better impedance matching (Balanis 2016). Microstrip feeding is also very convenient when it comes to fabricating an array of printed antennas to improve antenna performances such as directivity and gain.

2.3 Array Antenna

An antenna array can deliver more features that cannot be achieved using a single element antenna. Arrays are well known for attributes such as increased gain, and the ability to steer the radiation beam by feeding signals

of varying phase to individual elements of the array (Bashri, Arslan et al. 2015). Arranging individual elements in an array brings more degrees of freedom in terms of position. Thus, the geometrical configuration is the first thing that comes up while designing an array. A linear array is one where all elements are in the same row. If the elements are distributed in a plane rather than a single dimension, then the geometrical orientation of the array is called a planar array. Rectangular and circular orientation are the best examples of a planar array. Non-planar arrays like cylindrical and spherical are also used in specific applications, for example space communication.

The second important thing in an array antenna is the relative placement of individual elements. The distance between individual elements plays a vital role in array performance as the elements collectively contribute to radiation and mutually couple one another. The third thing to keep in mind while designing an array antenna is the excitation of discrete components in terms of amplitude and phase. Variation in amplitude and/or phase while exciting elements of an array is very handy for shaping and steering the beam. Scanning radars that detect aerial vehicles use this technique to scan the space, identify and get basic information like distance and shape of an aerial vehicle.

For arrays where all elements are identical, there are two almost independent variables that control the radiation pattern of the array. The first is called the *element pattern*, and the other is *array factor*. The array factor is the radiation pattern shown when the array is made of ideal isotropic elements. The total radiation pattern $E(\text{total})$ is given by following equation (Balanis 2016):

$$E(\text{total}) = E(\text{single element}) \times \text{Array Factor} \quad (16)$$

2.3.1 Linear Array Factor

For any array with all elements identical, if we note 'd' as spacing between elements and ' β ' as the progressive phase difference between them, then the linear array factor is given below:

$$AF = \sum_{n=1}^N e^{+j(n-1)(kd\cos\theta+\beta)} \quad (17)$$

where " θ " is the angle made between the axis of the linear collection of antennas and the observation point in space where radiation characteristics are determined and n is number of elements for array. The term $kd\cos\theta + \beta$ is also collectively termed as relative phase (φ). Relative phase is then used to measure the phase difference (β) which is progressive in the elements of an array to direct the beam in desired angles in space. Generally, computer-controlled algorithms are used in association with phase shifters to achieve beam steering.

2.3.2 Planar Array Factor

When the elements on the array antenna are distributed in a plane rather than a particular direction, such an antenna system is called a planar array antenna.

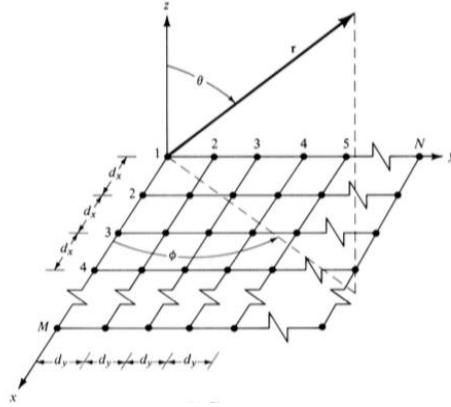


Figure 5: Planar array representation (Balanis 2016)

If “ dx ” and “ dy ” are the spatial separations between elements in X and Y directions as shown in Figure 10, then the array factor for such a system of elements is mathematically represented by:

$$AF(\theta, \phi) = A X B \quad (18)$$

$$A = \frac{1}{M} \frac{\sin\left(\frac{m\phi x}{2}\right)}{\sin\left(\frac{\phi x}{2}\right)} \quad (19)$$

$$B = \frac{1}{N} \frac{\sin\left(\frac{m\phi y}{2}\right)}{\sin\left(\frac{\phi y}{2}\right)} \quad (20)$$

where M and N represent the number of column and row in the array in Figure 10. Similarly,

$$\phi x = k dx \sin \theta \cos \phi + \beta x \quad (21)$$

$$\phi y = k dy \sin \theta \sin \phi + \beta y \quad (22)$$

where $k = \frac{2\pi}{\lambda}$ (wave number). The aforementioned equation is then used to identify the appropriate values of phase differences between adjacent elements for values of azimuthal angle “ ϕ ” and elevation angle “ θ ”, which will then identify radiation characteristics at any point in space surrounding this rectangular planar array antenna.(Balanis 2016).

2.4 Bio Radar Theory

In this bio-radar concept, electromagnetic (EM) waves are used to monitor the vital signs. It works on the principle of Doppler effect, in which a transmitter sends a signal and a receiver captures a signal with a change of phase and polarization upon reflection from a subject's body (Gouveia, Malafaia et al. 2018). Moreover, there is a change in the frequency of the signal due to micromovements of the subject's chest caused by breathing and heartbeat. The distance travelled by the radar signal can be represented by the number of wavelengths difference between the transmit (TX) signal and receive (RX) signal, which can be calculated as:

$$N\lambda = \frac{2R}{\lambda} \quad (23)$$

where R is distance between bio-radar and subject and λ is the wavelength. Under Doppler effect, if both the radar and target are fixed, then the received frequency would not change, as $N\lambda$ is constant. However, if the target is moving, either in the direction of radar or away from radar, the received frequency increases, and decreases, respectively (Boric-Lubecke, Park et al. 2015). This frequency shift is due to the change in wavelengths, which is in turn due to the change in distance, as with each wavelength there is a phase change of 2π . Hence, this phase change is dependent on distance R as:

$$\alpha = 2\pi N\lambda \quad (84)$$

In literature, radars can be generally classified into either continuous-wave (CW) or impulse radar. The latter is also known as ultra-wide band (UWB) radar. CW radar can be further classified into either unmodulated or frequency-modulated continuous-wave (FMCW) radar, as shown in Figure 1. CW and UWB also represent two common modes of operation of bio-radar for vital signs measurements. Figure 2 shows the corresponding waveforms.

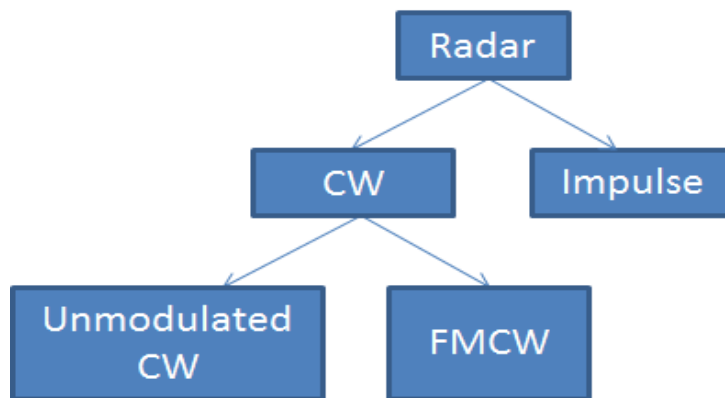


Figure 6: Radar types

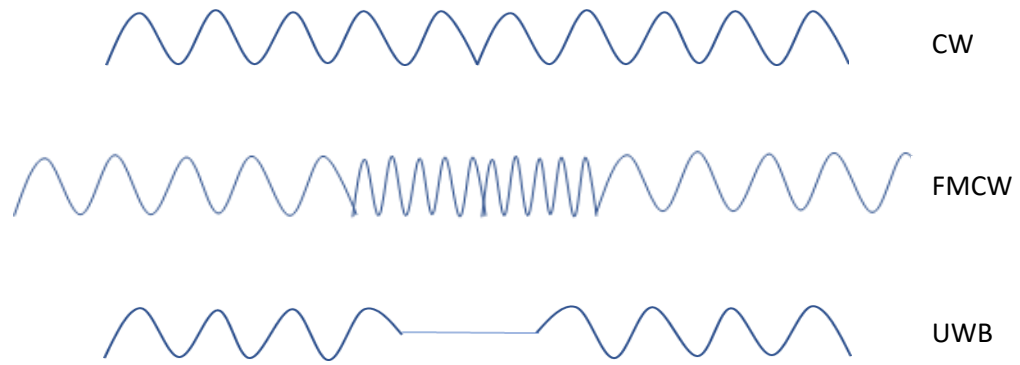


Figure 7: Modes of Operation of RADAR for Vital Sign Measurement

2.4.1 CW Radar

A narrow band single tone signal is transmitted and received in continuous wave CW radar. It can monitor and evaluate the velocity of subject's movements. This enables it to differentiate between a moving and stationary target, within its range (Skolnik 2008). The signal processing system is simple because of narrow band signals. However, there might be an interference of signal from transmitter to receiver side due to some signal leakage. Moreover, there could be reflections of other immovable objects in the vicinity, which can interfere with the received signal, leading to low signal-to-noise ratio.

2.4.2 FMCW Radar

FMCW can monitor distance and velocity between the radar and target, which is not the case with CW radar. Here, a triangular modulation is used to vary the signal frequency linearly with respect to time, and another triangular modulation is used with the received signal. The delay time between the received and transmitted signals is given by:

$$T = \frac{2R}{c} \quad (25)$$

where c is the speed of light. The signal bandwidth of the modulated signal detects the range, and the rate of modulation determines the range ambiguity (Skolnik 2008). The frequency difference between TX and RX signal in FMCW is due to the target movement. Hence, through this distance, the vital signs can be extracted.

2.4.3 UWB Radar

This radar works on principle of UWB communication. Here, short unit pulses are generated as the transmission signal which leads to a wide band signal. For a signal with a bandwidth of more than 500 MHz, it is considered to be a ultra-wide band signal (Boric-Lubecke, Park et al. 2015). These transmitted short pulses are reflected back by the target, and the distance between the radar and target ΔR can be calculated as (Kardo-Sysoev 2003):

$$\Delta R = \frac{c}{2 \cdot BW} \quad (26)$$

where BW is the bandwidth of the radar pulse. The distance-to-target D_t is given by:

$$D_t = \frac{c\Delta t}{2} \quad (27)$$

where Δt is the time delay between the TX and RX signals.

2.5 HR and BR Measurement

The measurement of vital signs such as heart rate (HR) and breathing rate (BR) are due to the tiny movements of heart and lungs, which lead to the movement of chest. The tiny movements of chest can be monitored using radar using microwave frequencies (Obeid, Sadek et al. 2011), which can penetrate through walls and obstacles (Huey-Ru, Chen et al. 1991). In the sequel, the concept of chest motion and the method to determine the HR and BR are presented.

2.5.1 Chest movement

Microwave Doppler radar signal is used to measure the chest movement. The signal is transmitted through an antenna onto the human chest, which is then reflected with the information of the chest displacement due to the heart beat and respiration.

A. *The Cardiac Cycle*

Heart beat is produced due to the pumping of blood in the whole body. The blood carries oxygen and energy to the cells. The cardiac cycle has a sequence of events through pulmonary and systemic circuits. There are two main episodes of the process: diastole and systole. The events of the cardiac cycle to pump in and out of the blood from itself happens in phases.

The period of contraction and pumping is called systole; while that of relaxation and filling is called diastole. In diastole phase, ventricle of the heart expands and the blood is filled. In systole phase, the ventricle contracts and the blood are pumped out of the heart. These two phases constitute one cycle of the heart. These phases occur simultaneously in both atria and ventricle parts of the heart. The cardiovascular system is the complete process to transport nutrients and the oxygen to the body tissues and extract waste from the cells. In this process, the heart is the muscle to do the pumping of the blood and the blood vessels act as the transporters (Bailey 2019).

The first event of the cardiac cycle is isovolumic convulsion of ventricles which leads to the closing down of the aortic and pulmonic valves. Due to the contraction, the pressure in the ventricle rises due to the tension developed. This increased pressure will close the mitral valve and tricuspid valve. The second event is ventricular expulsion, which will open the aortic and pulmonic valves, and the blood is ejected out of ventricular. This ejection happens due to the increased pressure inside the ventricle. The third event is isovolumic tranquillity, where the blood is filled in the atria and the step is called atrial diastole. This happens due to the reduction in ventricular pressure than aorta and closure of aortic and pulmonic. In the fourth event, the atrial pressure is increased by ventricle pressure and the valve gets opened. However, the blood flows into ventricles up to 70 % of its volume. The fifth

and final event takes place when the rest of 30 % blood is supplied to the ventricles in the atrial systole for each heartbeat.

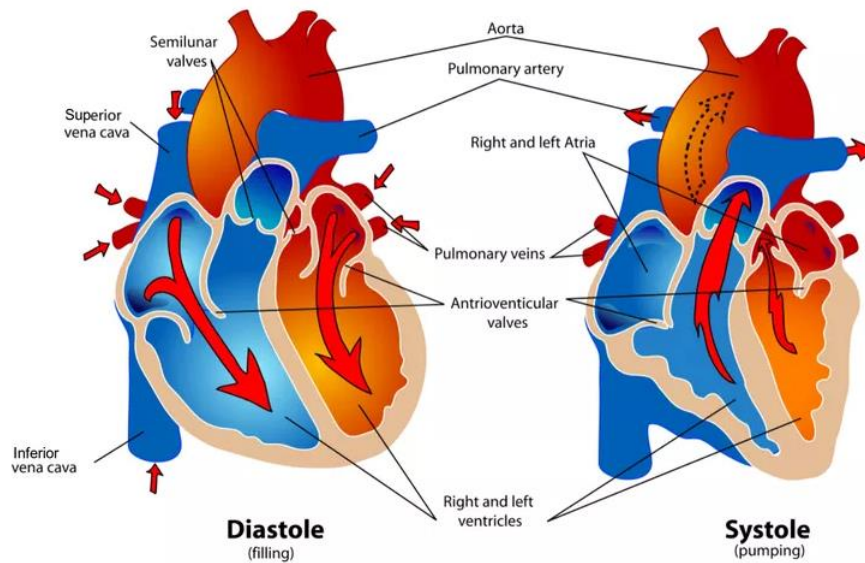


Figure 8: Heart anatomy and episodes of heart beat (Boric-Lubecke 2015, Park et al. 2019)

The process of simultaneous reduction and enlargement of heart leads to the movement of chest. The ventricle is responsible for the transport of blood to the tissues in body, resulting in large chest movement (D. Obeid Sept. 2010). Moreover, the contraction changes the shape of the heart which adds to more displacement on the chest walls (Samad 2017). The minimum movement in the chest is when the ventricular ejection is taking place. However, the average displacement of chest in one heart beat is 0.2mm to 0.5 mm (Ramachandran, Swarnamani et al. 1991).

B. Electrocardiogram

An electrocardiograph (ECG) is the measure of electrical activity of the heart. The expansions and contractions of the heart develops leads to the pumping of blood. The pumping in and out of the blood can be related to an electrical signal which can be measured by an ECG. The ECG is produced in form of a graph as shown in Figure 4, in which the different sections of the graph (P, Q, R, S, T, U) represent different events of the heart beat as explained earlier. The first peak 'P' is created due to the left and right atria, the upper section of the heart. Then there is flat line which is followed by an electrical pulse 'R' with the base of Q and S, are produced by the ventricles. The final pulse 'T' is an electrical recovery of the heart to a rest state for ventricles (Ian 2018).

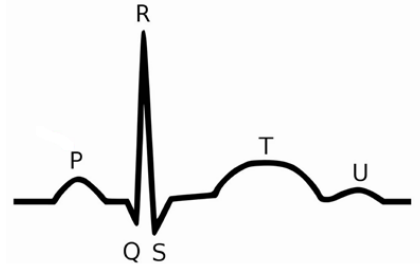


Figure 9: ECG output

2.5.2 Respiratory rhythm

The respiration is a two-step Quasi periodic activity which involves inhalation and exhalation, i.e. the inhalation of oxygen from atmosphere and the exhalation of carbon dioxide into atmosphere. The contraction of muscles is caused by the thorax due to the exchange of gas in lungs. This contraction is caused by the pressure differences in thorax and external atmosphere. The movement of this air to and from the lungs causes motions of the chest region including ribcage, abdomen and thorax. This motion cause displacement on the outer surface of the skin. This displacement is measured by the Doppler effect through a bio-radar. The BR is a key vital sign for human being as it provides information regarding the condition of the patient (Fletcher and Jing 2009). For a normal healthy adult, BR should be between 12–20 times per minute and the chest displacement should be same in each breath (Tan and Hoole 1998).

2.6 Doppler Radar

This radar uses Doppler effect to find the velocity of objects at a distance. In this thesis, Doppler radar is similarly used to measure the vital signs of a human body. A signal is transmitted and received through an antenna. The received signal consists of the information regarding the displacement of chest due to heart beat and breathing. This radar system consists of pair of antennas for transmitting and receiving signal and a processing algorithm to detect the displacement of chest (Tan and Hoole 1998, Das, Boothby et al. 2012).

The phenomena of a frequency change in the received signal due to the movement of source at the observed point is known as *Doppler Effect*. The observed signal frequency at the observation terminal can be expressed as (Schäfer, Diewald et al. 2018):

$$f = \frac{c+v_r}{c-v_s} f_o \quad (28)$$

where c is medium velocity, f_o is operating frequency, v_r is velocity of receiver, and v_s is velocity from source relative to medium. The source velocity can be positive or negative. It is considered positive when the source and observer are coming close, and is considered negative when the two are getting away. However, if the source is not moving, the change in frequency observed can be re-expressed as:

$$f = \frac{c+v_r}{c} f_o = (1+\frac{v_r}{c})f_o \quad (29)$$

The Doppler shift is defined as:

$$f_d = f - f_o \quad (30)$$

Hence, f_d and f_o are related by:

$$f_d = \frac{v_r}{c} f_o \quad (31)$$

If the source of radar is also the observer, the Doppler frequency observed by the radar is given by:

$$f_d = \frac{2v_r}{c} f_o \quad (9)$$

since relative velocity is doubled. If the source and observer are not collinear and there is an angle θ between the two as shown in Figure 5, the relative velocity can be expressed as $v_r = v_a \cos \theta$ where v_a is original velocity.

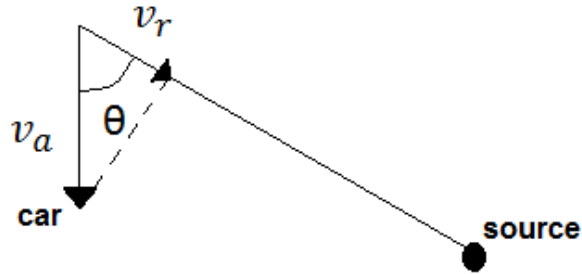


Figure 10: Doppler Effect

2.7 Literature Review

This section discusses related works on antenna designs for radar applications. The discussions are categorized by the antenna requirements of applications, namely directivity, frequency, compactness, polarization, and flexibility requirements.

2.7.1 Directivity

Higher the antenna directivity or gain, higher the signal-to-noise ratio and more accurate measurement by the radar signals. In (Das, Boothby et al. 2012), the authors evaluated different 2.4 GHz antennas for vital signs monitoring, including patch, helical and Yagi-Uda antennas. The patch antenna exhibits a half-power beamwidth of 92° and a promising performance for vital signs detection. A helical antenna operating in axial mode at 2.4 GHz for a Doppler based CW radar is presented in (Boothby et al. 2012). It is an 8-turn design with on-reflector impedance matching to maintain the size. Compared to a conventional 2.4 GHz patch antenna, the helical design can offer a higher gain.

However, the planar nature of the patch is attractive to achieving low profile and ease of fabrication using printed circuit board (PCB) technology. To improve directivity, multi-element array and higher operating frequency can be used by the patch design. For a given antenna size, a higher frequency narrows the beamwidth due to a larger size-to-wavelength ratio, resulting in higher directivity. The narrower beamwidth allows the antenna aperture to focus towards the human subject for both transmission and reception, thus avoiding interference from environmental clutter and noise.

Although high directivity is often desired in radar applications, there are times when antennas with a wide beamwidth is needed to gather information from a wide vicinity. For instance in (Schäfer, Diewald et al. 2018), a system of three series-fed 24 GHz patch antennas was deployed on a ceiling to monitor vital signs of elderly people as they move freely around the room.

2.7.2 Frequency

Radar modules can be designed for low, intermediate and high frequency. In (Shen et al. 2012), a 60 GHz circularly polarized 2×2 patch antenna array was implemented on low-temperature co-fired ceramic (LTCC) substrate and was integrated with a Doppler radar system. In (Lan et al. 2015), a 24 GHz millimeter wave antenna was designed to monitor the vital signs of patients who are immovable and in mental stress. Another design operating at 77 GHz proposed by the same authors in (Lan et al. 2016) is a linear array with ten small patch antennas connected with quarter wave impedance transformers to reduce sidelobe levels. A 915 MHz fractal antenna used with a low noise amplifier was proposed for continuous wave (CW) Doppler radar to monitor heart

rate and breathing rate (Park et al. 2019). However, the use of low frequency limits the achievable antenna compactness and detection sensitivity when operating in a near-field condition. On the other hand, the use of high frequencies can make bio-radar sensitive to subtle movements of the subject, such as chest wall micromovements due to heart beat.

2.7.3 Compactness

The compactness of antenna can be an important factor for some radar applications such as when the radar unit needs to be implemented on a portable device. A compact-size antenna can be achieved by designing it to operate at a high frequency, e.g. at high microwave or millimeter wave frequencies. Operating at a high frequency can also reduce the spacing between two antennas of the radar system (one for transmit; one for receive), which must be at least a half wavelength to avoid mutual coupling.

A more compact radar system can also be achieved by using only one antenna for both transmit and receive as reported in (Jeong-Guen et al. 2005, Chuang et al. 2012, Bo et al. 2016). However, in such systems, circulators are often used to separate the transmitted and received signals, which are not compact in size and also expensive. An alternative is couplers as used by (Gu et al. 2019), but they divide signal power and add to insertion loss, rendering the radar system more prone to noise and interference.

In (Rabbani and Ghafouri-Shiraz 2017), a comparative analysis is performed on a bio-radar using single antenna and two antenna designs. The results showed that while performance of the single-antenna system is good, the detection range is somewhat limited. On the other hand, the performance of the two-antenna system is good without the drawback of a limited range. Hence, for applications where long detection range and compactness are both essential, the key challenge is to design a two-antenna radar system with relatively small foot-print.

2.7.4 Polarization

Compared to linearly polarized antennas, circularly polarized antennas are generally preferred in radar applications as the transmitter and receiver signals can be more easily isolated. This will also reduce higher order reflections and improve isolation from multiple reflections. Large ferrite device and circulator which are commonly used to isolate transmitter and receiver signal can thus be avoided. In (Boothby, Hwang et al. 2012), authors performed an analysis of circular polarization for bio-radar setup. Three antennas: one transmitter antenna that is right-hand circularly polarized (RHCP); and two receiver antennas, one RHCP and another left-hand circularly polarized (LHCP). The transmitted signal is reflected through a metallic reflector and the received signal is measured at both receiver antennas. It was found that the antenna pair with opposite polarization is more efficient than the pair with similar polarization. In (Chan et al. 2013), the authors designed

a circularly polarized antenna for vital signs monitoring that provides a more stable radar cross-section (RCS) of the human subject than a linearly polarized antenna due to scattering effect that varies with the material, thickness, shape, and size of the target object. In (Changzhi and Jenshan 2008), the authors proposed a signal reformation method that utilizes different antenna polarization. This was used to omit null detection point, which is a key challenge in contactless vital monitoring due to the noise generated by random body movements.

2.7.5 Flexibility

Flexibility is another upcoming property of the flexible circuits for next-generation consumer electronics. The materials used may include soft plastics, textiles, or even paper to make conformal antennas that can be easily integrated onto non-planar surfaces (Chen et al. 2018) such as spherical, cylindrical, and other complex shaped surfaces. In (Mustafa and Rajendran 2019), the authors designed a 2.45 GHz wearable antenna using flexible material to measure human vital parameters. The materials include fabrics, telfon, rubber, and paper. In (Zahran & Gaafar 2017), the bending effects on a flexible ultra-wide band antenna on liquid crystal polymer substrate were studied. It demonstrated the antenna's ability to maintain its radiation pattern and gain performance under various bent conditions. However, these are wearable antennas that operate in near-field conditions. To the best of our knowledge, the flexibility feature has not been explored by bio-radar systems that operate in the far-field for vital sign monitoring.

2.8 Summary

This chapter provides the background theories on antennas, bio-radar systems, and measurement of vital signs such as heart rate and breathing rate. This chapter also reviews the existing literature on antenna design for radar applications and only a handful are found to be designed for a bio-radar system for noncontact human vital signs monitoring. The findings from the above review motivated us to propose a bio-radar antenna with the following features: (i) high operating frequency (24 GHz) for a compact two-antenna design; (ii) circularly polarized for high isolation between transmitter/receiver signals; (iii) high directivity with low-profile using multi-element patch array design; and (iv) flexibility to allow mounting on non-planar surfaces such as curved walls and edges. The research methodology to be followed is discussed in the next chapter.

Chapter 3: Research Methodology

3.1 Antenna Design and Simulation

Antenna design is basically an optimisation process in which different structural and material elements of the antenna influence the antenna's behaviour. The first step to designing an antenna is simulation. The antenna design and simulation software used is the AnSys High Frequency Structure Simulator (HFSS) which employs finite element method (FEM) for full-wave electromagnetic (EM) field simulation of 3D passive structures such as antennas. It integrates 3D modelling of antenna structure, performance simulation of the antenna, and performance visualization through 2D reports and field plots.

3.2 Antenna Fabrication

The fabrication requires firstly exporting the HFSS model of designed antenna to an AutoCAD DXF (Drawing Interchange Format) data file, which is then used for fabricating the antenna. The fabrication methods explored in this thesis included laser cutting and conventional lithographic technique. The flexible substrate used for the designed antennas is Panasonic R-F705S liquid crystal polymer (LCP) of 100 μm thickness and permittivity ϵ_r of 3.35.

3.2.1 Laser Cutting

Initially, the laser cutting approach was explored. A thin and flexible layer of copper foil with adhesive backing is firstly attached on the liquid crystal polymer (LCP) substrate. Then, the desired antenna pattern is laser-cut and excess copper is removed. While the quality of laser-cut pattern is good, removing the excess copper is difficult without damaging the finer parts of the pattern. As a result, another approach was taken: the copper foil is firstly laser-cut and then the cut pattern is peeled off and transferred to the substrate. While this approach is successful in preserving the pattern, it is difficult to avoid any misalignment of the pattern on the substrate during the transfer process, resulting in some changes to the antenna's behaviour.

3.2.2 Photoetching

Due to aforementioned issues with laser cutting, a different approach based on conventional lithographic technique or photoetching is used. It is an electro-chemical way of removing unwanted parts of the copper-clad LCP substrate to produce the antenna pattern. As the quality of the photoetched sample is good, this method is adopted for fabricating all the antennas designed in this thesis.

3.3 Antenna Characterization

The Anritsu S802E Site Master is used as the vector network analyzer (VNA) for characterizing the fabricated antennas. The key attribute measured is the S_{11} parameter for the antenna's return loss, and S_{21} parameter for the antenna's gain and vital signs measurement.

Before the measurement, it is necessary to firstly calibrate the VNA at the sweeping range of interest, e.g. 22-26 GHz. The calibration is performed in three steps, commonly referred to as the three-point calibration method. It is done using a calibration kit with three types of load attachment:

- Open circuit $Z_L = \infty$ (theoretically $\Gamma = 1$)
- Short circuit $Z_L = 0$ (theoretically $\Gamma = -1$)
- Perfectly absorbing load $Z_L = Z_0$ (theoretically $\Gamma = 0$)

3.4 HR and BR Signal Acquisition

The setup for heart rate (HR) and breathing rate (BR) measurement is shown in Figure 11. Two designed 24 GHz antennas: one for transmit (TX) and one for receive (RX), are positioned with their radiating patch facing the chest area of a human subject sitting approximately 60 cm away. The TX and RX antennas are connected to Port 1, and Port 2 of the VNA, respectively, using coaxial cables each of approximately one meter long. Each antenna is interfaced with the coaxial cable using a SMA connector with a specified maximum operating frequency of 26.5 GHz.

The VNA is setup to measure the S_{21} parameter, which represents the signal reflected from the human subject detected by the RX antenna relative to the incident signal transmitted by the TX antenna. For HR and BR measurement, knowing the phase of S_{21} is the most important, as the phase variation provides information regarding the chest displacement, which is in turn used to determine the cardiopulmonary activity (Obeid, Zaharia et al. 2012).

The VNA is configured with an intermediate frequency bandwidth (IFBW) of 100 Hz and generates a continuous wave of 24 GHz. For an IFBW of 100 Hz, the time for one measurement cycle is 18 seconds, during which 2048 signal samples are collected. Under Doppler effect, the received signal will have a time-varying phase change with respect to the transmitted signal. This phase change $\Delta\theta(t)$ is due to chest displacement $\Delta x(t)$, which can be found by:

$$\Delta\theta(t) = \frac{4\pi}{\lambda} \Delta x(t) \quad (33)$$

where λ is the wavelength of transmitted signal (Obeid, Zaharia et al. 2012). The obtained S_{21} data is then processed using a MATLAB program to extract the HR and BR information.

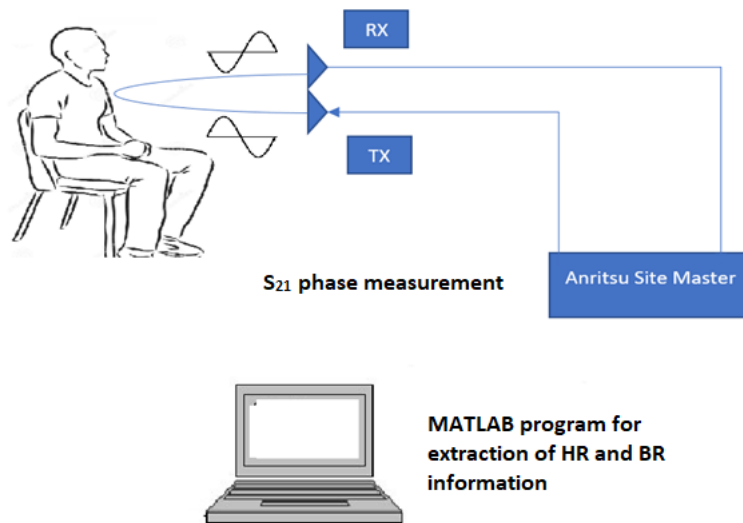


Figure 11: Setup for HR and BR measurement

3.5 HR and BR Signal Processing

In this section, the signal processing, filtering, and smoothing model is presented to extract the HR and BR values from the S_{21} phase measurements, which contain information about the chest displacements due to heartbeat and breathing activity. The chest displacement due to breathing and heartbeat is between 4–12 mm, and 0.2–0.5 mm, respectively. On the other hand, the frequency of breathing and heartbeat in a normal adult is between 0.2–0.34 Hz, and 1–2 Hz, respectively. This translates into 12–20 breaths per minute, and 60–120 beats per minute, for a normal adult.

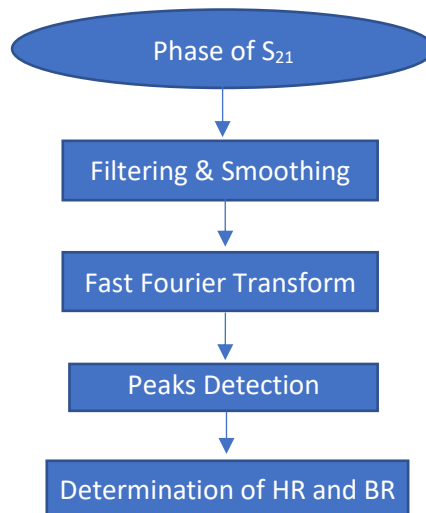


Figure 12: Signal processing steps to determine HR and BR

The signal processing model is implemented in MATLAB, which performs filtering and smoothing of data, Fast Fourier Transform (FFT) to convert time-domain phase signal into frequency domain, and peak detection in the frequency spectrum to determine the HR and BR, as shown in Figure 12. The heartbeat and respiration rates are obtained by applying fast Fourier transform (FFT) to the original signal. The dominant peak in the frequency domain was taken as the breathing frequency, and the second dominant peak was taken as the heartbeat frequency. The following sub-sections briefly describes each of these processing steps.

3.5.1 Fast Fourier Transform

FFT is performed on the received phase signal to convert it from a time-domain signal into a frequency-domain signal in order to extract the HR and BR values. For a given n number of complex inputs $x_0 \dots \dots x_{n-1}$, their discrete fourier transform (DFT) can be expressed as:

$$y_k = \sum_{0 \leq l < n-1} w_n^{kl} x_l \quad 0 \leq k < n \quad (34)$$

where $w_n = e^{(-\frac{2\pi i}{n})}$ and $i = \sqrt{-1}$ (Rao 2001). DFT takes a discrete signal in the time domain and transforms that signal into its discrete frequency domain representation. Hence, it is able to determine characteristics of the signal in the frequency domain.

3.5.2 Filtering

Filters are applied to the signal to remove any undesired elements so that the desired data can be extracted. Filtering process can be done using an analog filter or a digital filter. Analog filters contains actual electronic physical circuits, which consists of resistors, capacitors, inductors or Op- Amps to receive desired signal output (Dwivedi 2015, Srinivasan and Gopalakrishnan). On the other hand, digital filters are mathematical operations performed on the sampled signal to filter out any unnecessary data. Since the received signal from the human subject are discrete time signals, digital filters have to be used. The difference equation for digital filter can be expressed as:

$$y_n = \sum_{k=1}^N a_k y(n-k) + \sum_{k=0}^M b_k x(n-k) \quad (35)$$

or by a system function:

$$H(z) = \frac{Y(z)}{X(z)} = \frac{\sum_{k=0}^M b_k z^{-k}}{1 - \sum_{k=1}^N a_k z^{-k}} \quad (36)$$

where a_k and b_k are filter coefficients, and x and y are input signal, and output signal, respectively (Smith 1997). Figure 13 shows the magnitude response of a typical filter ((Changzhi and Jenshan 2008).

3.5.3 Smoothing

The smoothing strategy is based on moving average, in which a sample point of a frequency-domain signal is replaced by an average of itself and surrounding points. Thus, if we consider X as a signal vector with N number of sample points, i.e. $X = (X_0, X_1, X_2, X_3, \dots, X_{N-1})$, then the sample point i of the smoothed signal $X_s(i)$ is expressed as:

$$X_s(i) = \frac{1}{n} \sum_{k=i-m}^{i+m} X(k) \quad (37)$$

where $n = 2m + 1$ is the smoothing window length. For odd values of n , i lies between n and m .

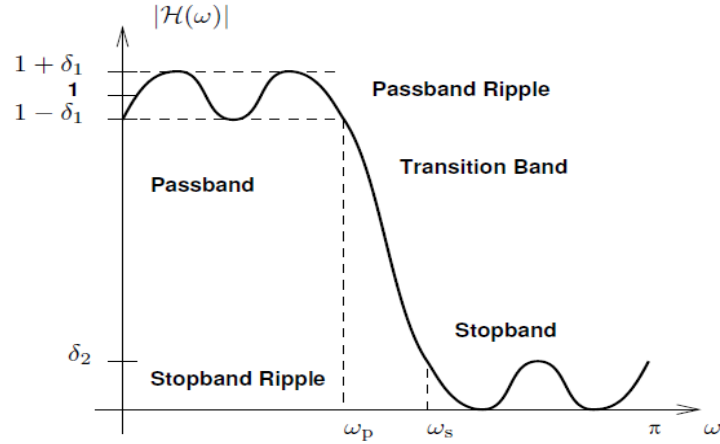


Figure 13: Magnitude response of a typical filter

3.5.4 Peak Detection

The detection of peaks in the FFT frequency spectrum is the technique used for determined both of our measured vital signs. Essentially, the frequency of the highest peak in the FFT spectrum between 0–0.34 Hz identifies the measured breathing rate (corresponding to 0–20 breaths per minute), while the frequency of the highest peak of the FFT spectrum between 1–2 Hz identifies the measured heart rate (corresponding to 60–120 beats per minute). It is also common to firstly convert the frequency range of 0–2 Hz into a vital signal range of 0–120 beats/breaths per minute prior to the peak detection.

3.6 Summary

This chapter describes the research methodology used in this work, including the use of the HFSS software for antenna design and simulation; laser-cutting and photoetching for antenna fabrication; VNA for antenna performance characterization and HR/BR signals acquisition from human subjects; and MATLAB software for HR/BR signal processing and value extraction. Using HFSS, three antenna designs for Doppler radar-based HR/BR monitoring are presented in the next chapter.

Chapter 4: Proposed Antenna Designs

Three circularly polarized patch antennas on flexible LCP substrate have been designed to operate at 24 GHz: (i) single-element unit cell; (ii) two-element array; and (iii) four-element array. The aim of increasing the number of elements is to improve the gain of the antenna. The initial square patch dimensions of the antennas are calculated, and then full-wave simulations are conducted using HFSS to optimize the design in terms of size and performance, resulting in an ellipse-shaped slotted patch unit cell. The two- and four-element array are then designed based on this optimized unit cell.

To achieve circular polarization, two orthogonal modes with closely separated resonant frequencies are generated. This results in a circulating current on the patch at a frequency between the two shifted resonant frequencies where the 90° phase difference condition is met. It is obtained by shifting the feed line from the center of the patch and by cutting two slots in the patch. The following sub-sections further describe each of the three designed antennas.

4.1 Single-element unit cell

The designed unit cell consists of a monopole patch, feed element, and ground plane as shown in Figure 14 with an overall dimension of 20×16 mm. The length of feed line is 3.6 mm, the ellipse-shaped radiating patch has a semi-major axis and semi-minor axis length of 5.86 mm, and 4.28 mm, respectively. Two slots measuring $0.5 \times 1.59 \times 1.37$ mm are cut on both sides of the horizontal ellipse. The copper thickness of the patch and ground plane is $18 \mu\text{m}$ as specified in the datasheet of the LCP substrate.

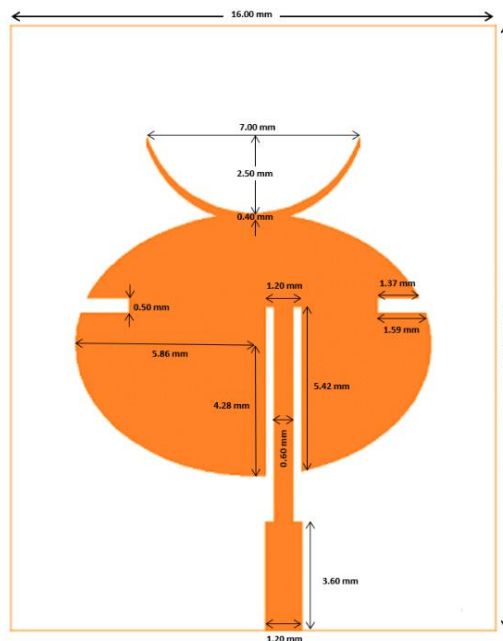


Figure 14: Single-element unit cell

4.2 Two-element array

To further improve the gain of the unit cell, arrays using multiple unit cell elements are designed. The designed two-element array is shown in Figure 15 with an overall dimension of 29.5×25.4 mm. The closest separation between the two elements is 1.6 mm. The feed line is a 50 Ω input, which is split into two 100 Ω lines to power each individual patch. Here, the T-shaped power divider is used along with a quarter wave transformer for impedance matching. The width and length of the feed element is 1.5 mm, and 10.2 mm, respectively.

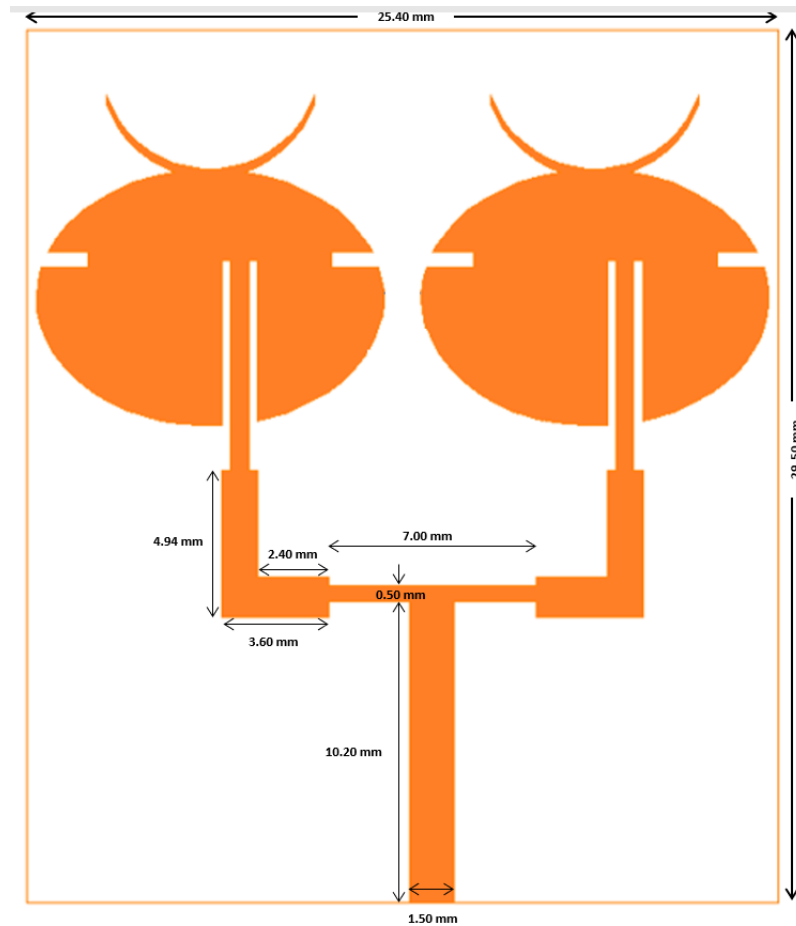


Figure 15: Two-element array

4.3 Four-element array

Similarly, a four-element array is designed with an overall dimension of 53×36.5 mm as shown in Figure 16. The inter-element separation is 1.6 mm. The width and length of the feed element is 1.5 mm, and 9.3650 mm, respectively. Figure 17 shows the fabricated antenna samples on flexible LCP substrate with a substrate thickness of 0.1 mm.

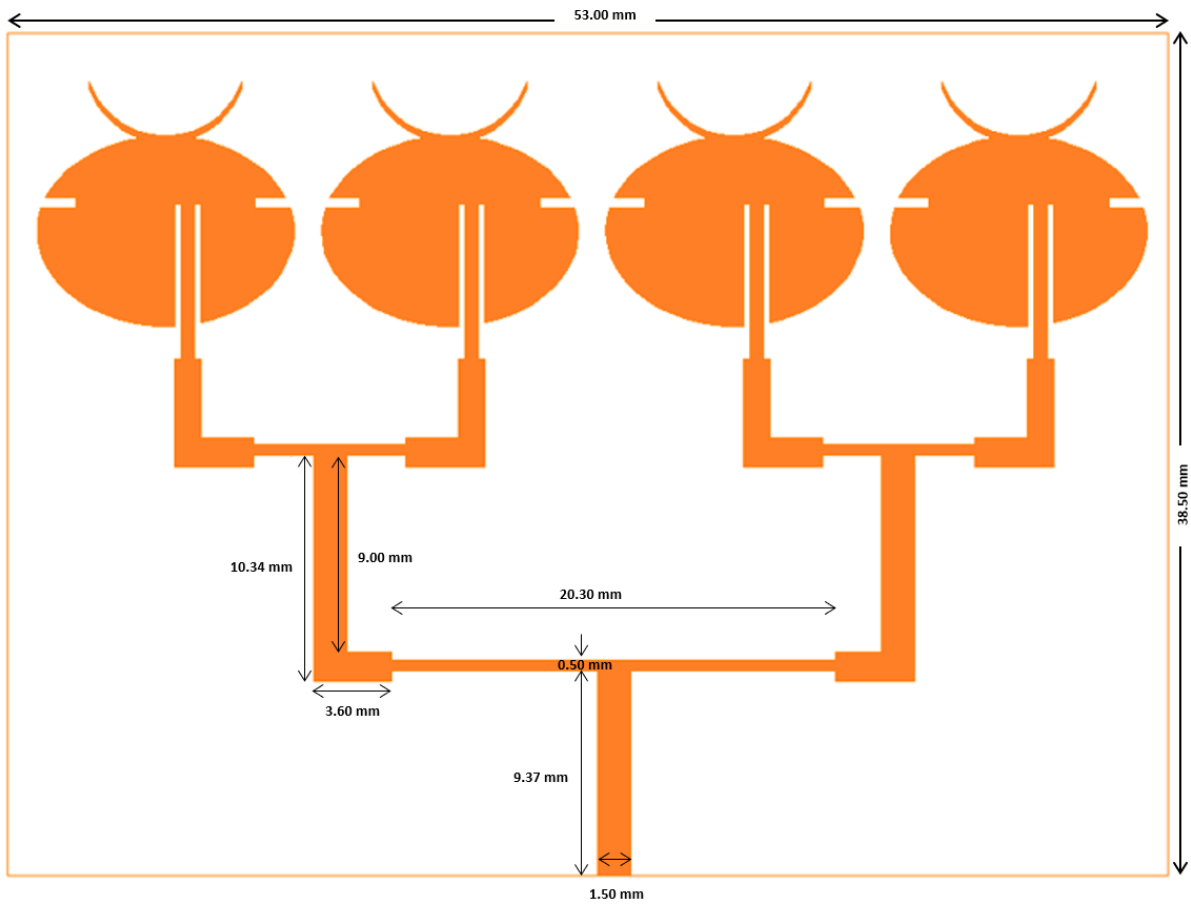


Figure 16: Four-element array

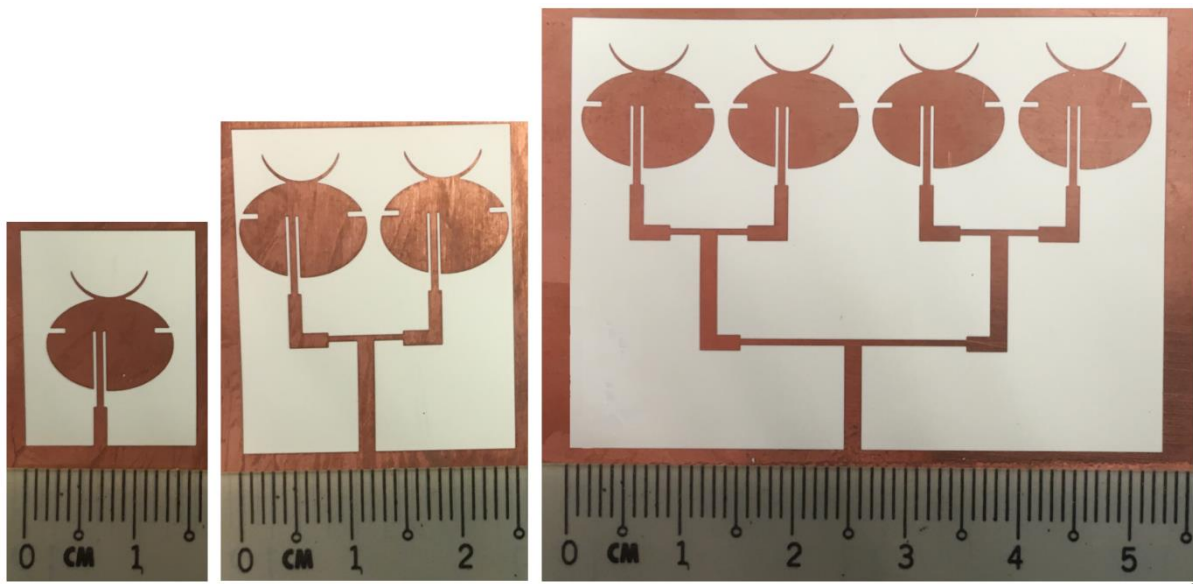


Figure 17: Fabricated antenna samples

4.4 Summary

In this chapter, a single antenna element (a.k.a. unit cell) on a flexible liquid crystal polymer (LCP) substrate for a 24 GHz bio-radar system is firstly designed. This is followed by the design of a 2- and 4-element array using the same unit cell to achieve better directivity and circular polarization performance for the bio-radar application. The final antenna prototypes were fabricated on copper-clad LCP substrate using photoetching. The performance analysis of both simulated and fabricated antennas is explained in the next chapter.

Chapter 5: Results and Discussion

5.1 Simulated Antenna Performance

The designed antennas in Chapter 5 are simulated using HFSS where a wave port is used for excitation. Each of the antennas: single-element unit cell, two-, and four-element array, are evaluated in terms of their return loss, radiation pattern, gain, and axial ratio performances.

A. Return Loss

The return loss is a measure of the impedance mismatch between the feed line and antenna. The lower the return loss, the less amount of power is reflected and lost through impedance mismatch, and the more power is delivered to the antenna. Figure 18 shows the simulated return loss $|S_{11}|$ for the proposed single element unit cell. It shows that the antenna achieves a return loss of approximately -16 dB at 24 GHz.

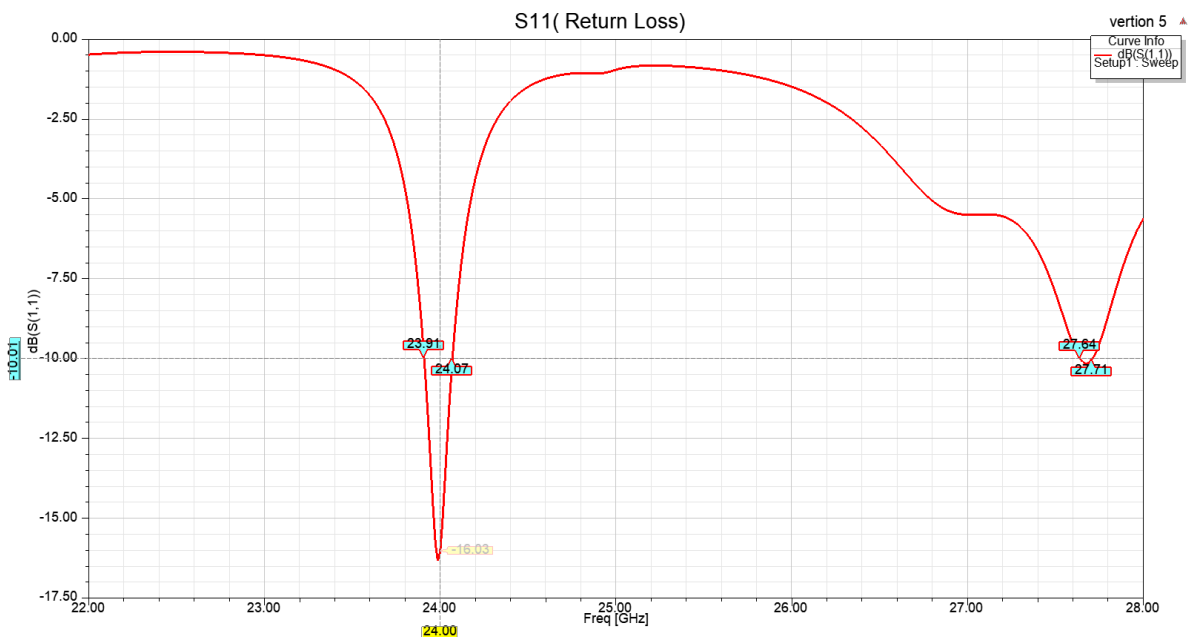


Figure 18 Single element return loss $|S_{11}|$

Figure 19 and Figure 20 shows an increasingly better return loss performance of -21.1 dB and -28.75 dB for the two-element, and four-element array, respectively. The latter also exhibits a -10 dB bandwidth of approximately 190 MHz.



Figure 19: Two-element array return loss $|S_{11}|$

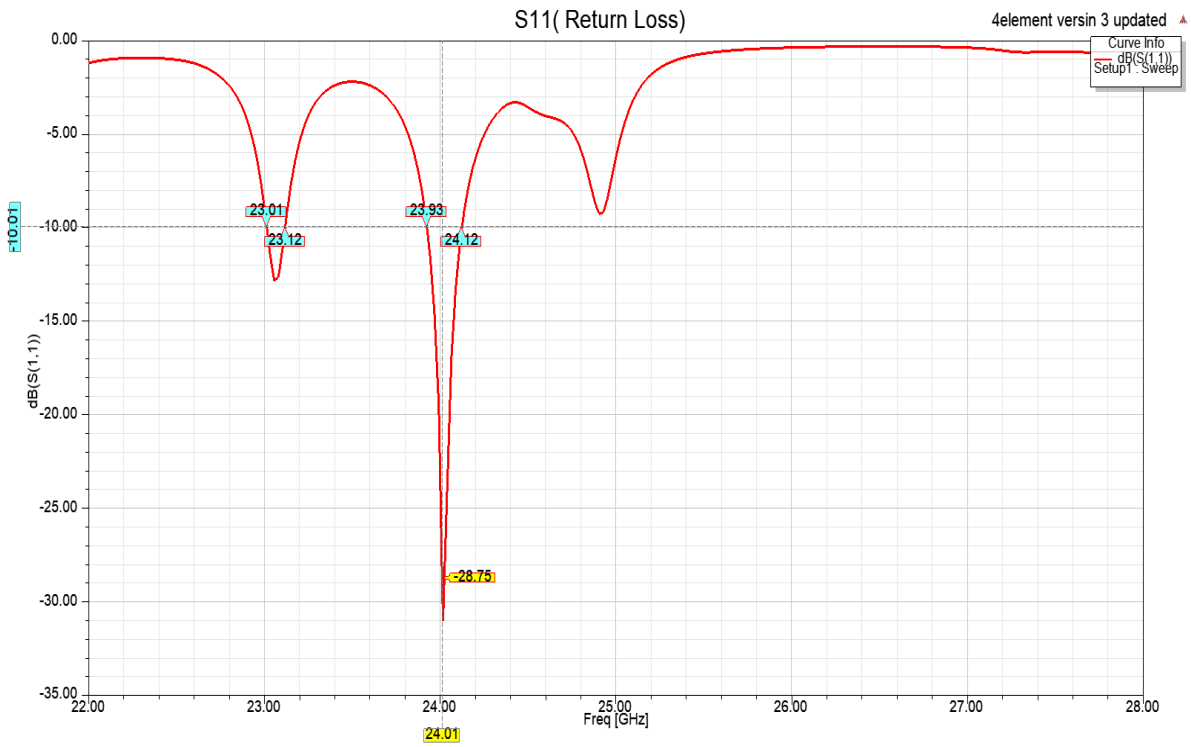


Figure 20: Four-element array return loss $|S_{11}|$

B. Radiation Pattern

The radiation pattern depicts how the radiated signal from the antenna varies in different directions. Figure 21 and Figure 22 shows the simulated radiation pattern, and the corresponding 3D polar plot, respectively, for each antenna. It shows the maximum radiation intensity is in the direction of $\theta=0^\circ$ for both element and array. Moreover, increasing the number of elements has the effect of narrowing the main beam.

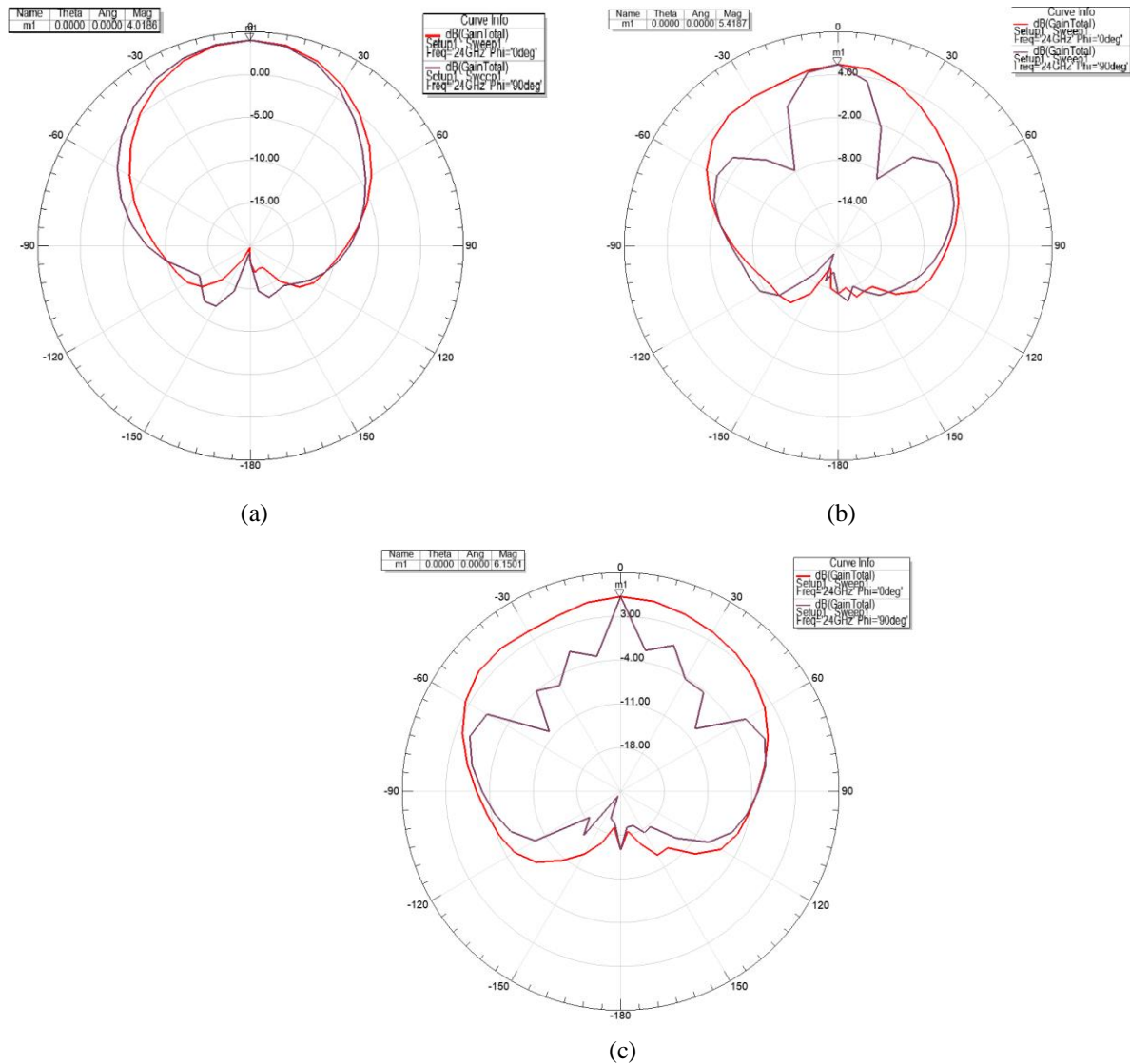


Figure 21: Radiation pattern of (a) single-element unit cell; (b) two-element array; (c) four-element array. The plot for $\varphi=0^\circ$ and $\varphi=90^\circ$ refers to the E-plane (side-view) and H-plane (top-view), respectively

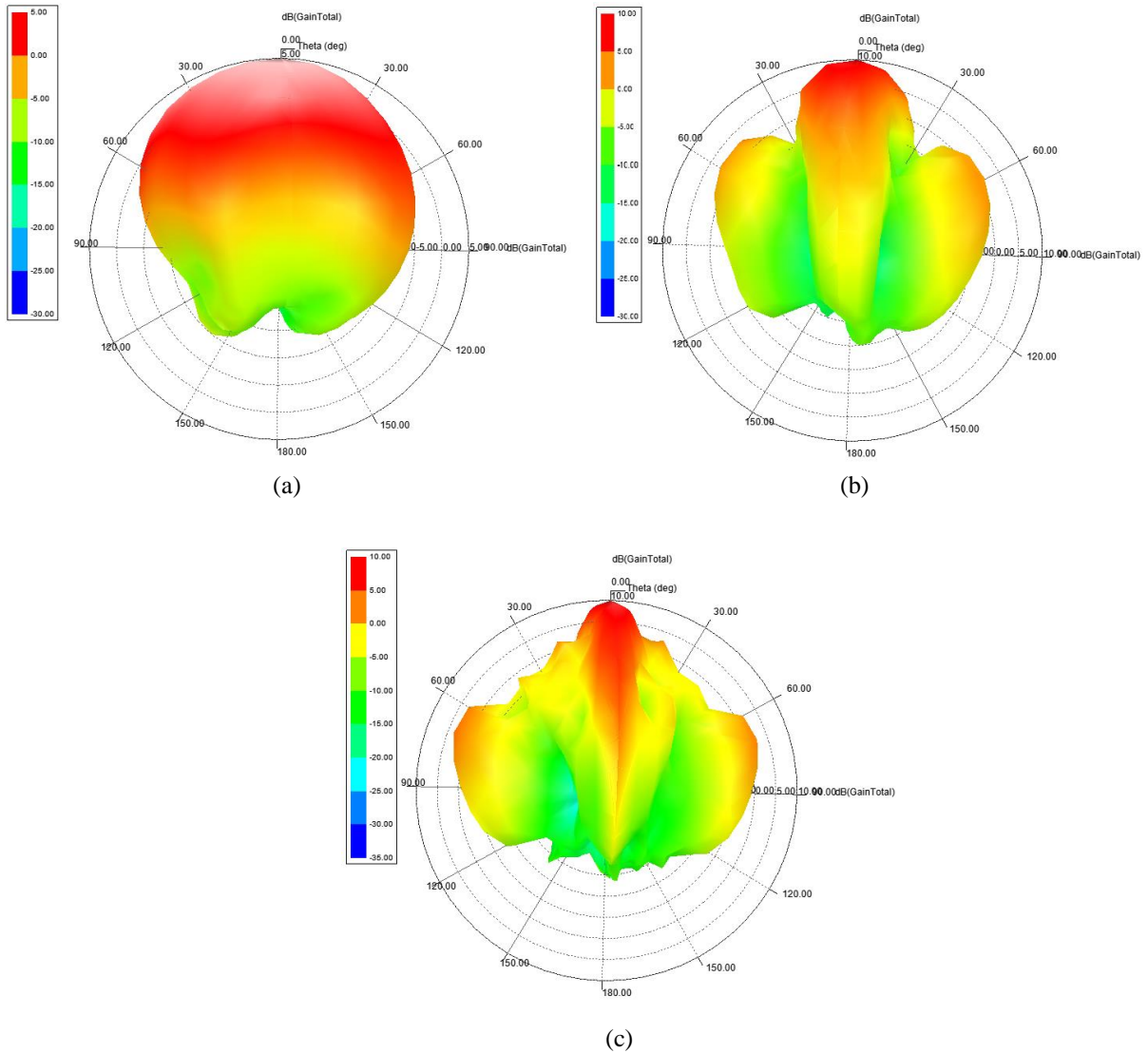
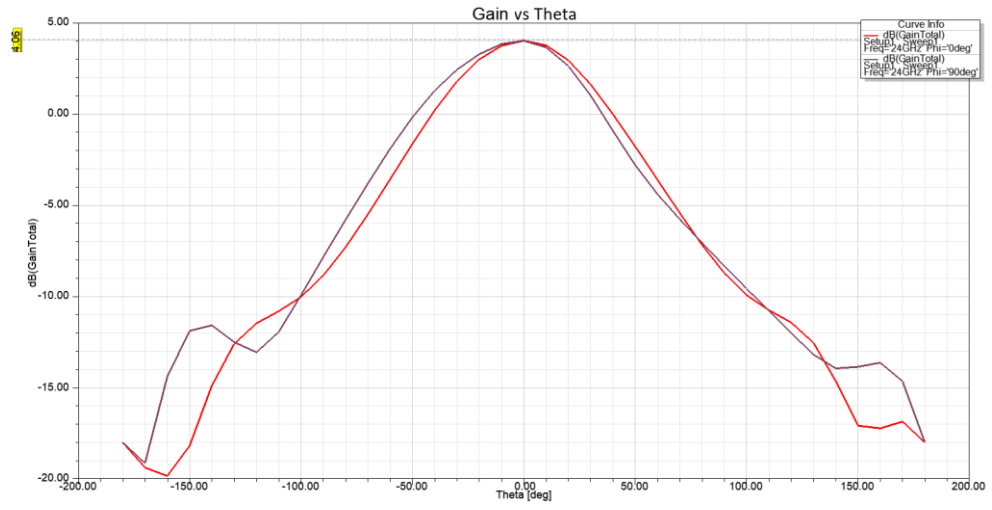


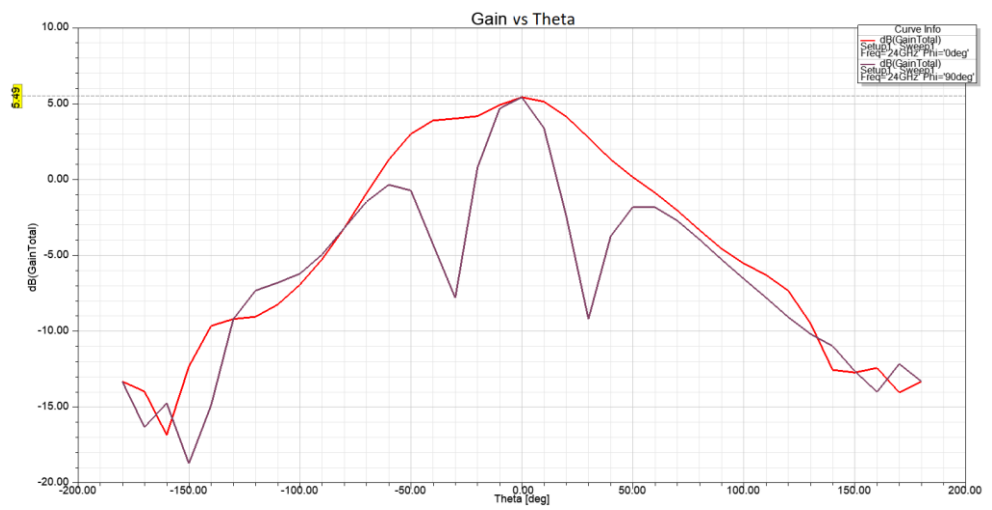
Figure 22: 3D polar plot for (a) single-element unit cell; (b) two-element array; (c) four-element array

C. Gain (Directivity)

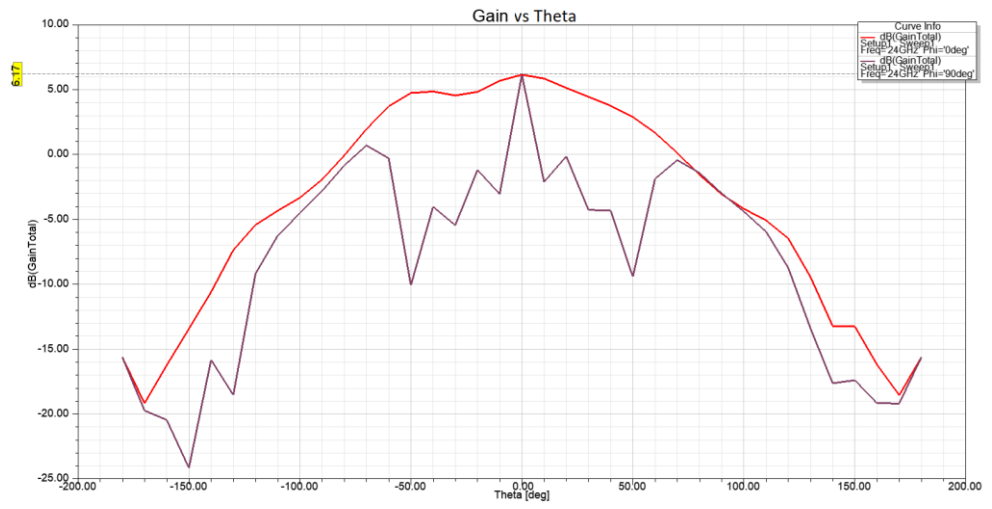
The gain is a measure of the antenna's directivity or extent to which its signal propagates in the peak direction of radiation. The simulated gain on E-plane ($\phi=0^\circ$) and H-plane ($\phi=90^\circ$) as a function of theta (θ) at 24 GHz for each antenna is shown in Figure 23. The results show a maximum gain of 4.09 dBi, 5.49 dBi, and 6.17 dBi, are achieved at $\theta=0^\circ$ on both planes for single-element unit cell, two-element array, and four-element array, respectively. The achieved gain is attributed to the added horn type structure to the basic elliptical design.



(a)



(b)



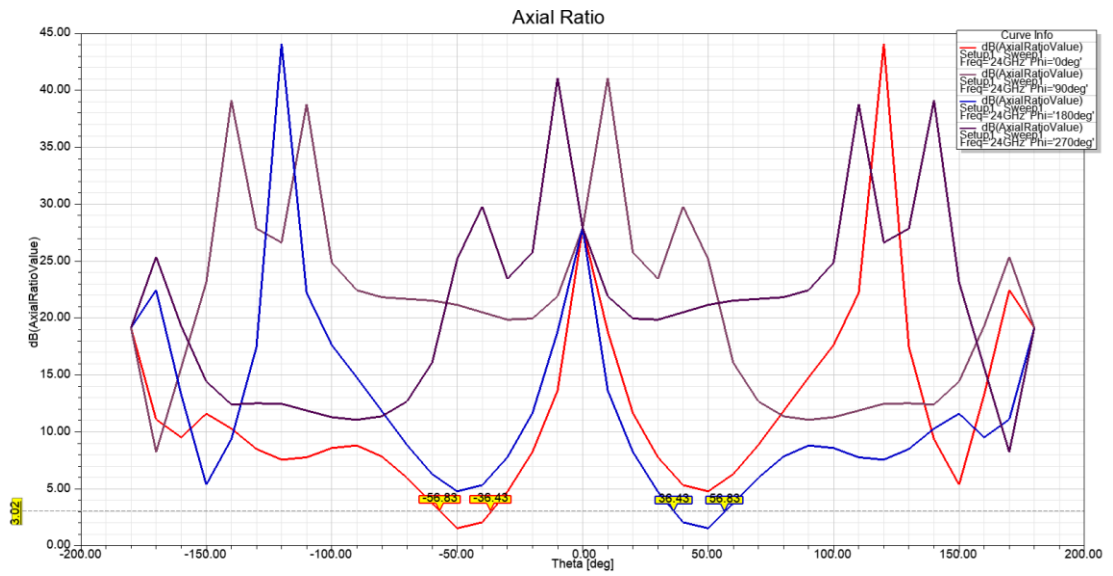
(c)

Figure 23: Gain versus Theta (θ) for (a) single-element unit cell; (b) two-element array; (c) four-element array, with $\phi=0^\circ$ (red) and $\phi=90^\circ$ (purple)

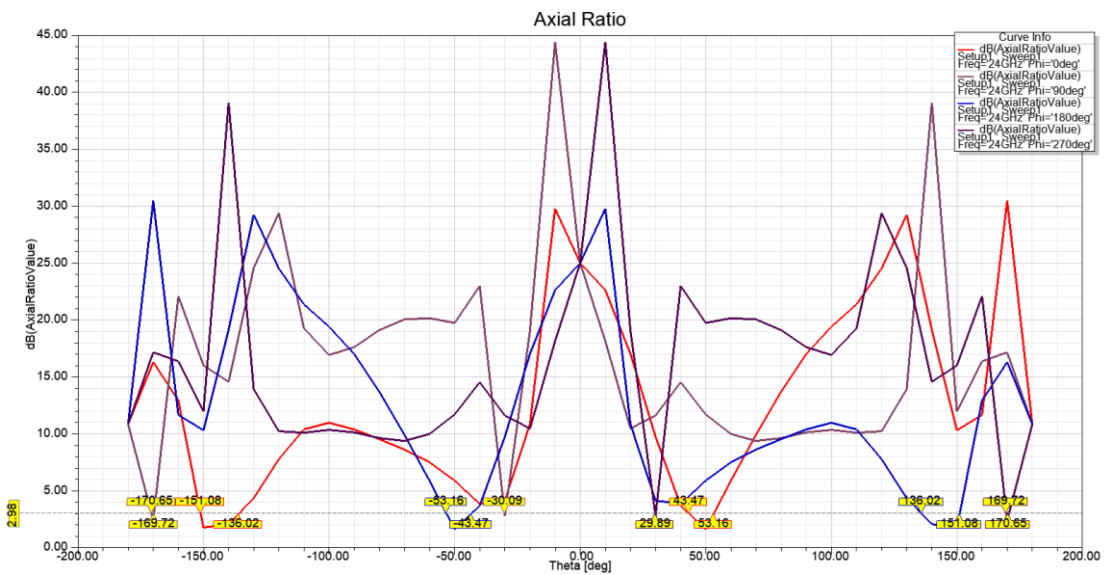
D. Axial Ratio

The axial ratio could measure how circularly polarized an antenna is. A perfectly circularly polarized antenna will have an axial ratio of 0 dB. However, an axial ratio of 3 dB or less is generally acceptable in practice. The proposed antennas are not fed from in between the ellipse, but rather towards the edge. This initiates two orthogonal modes (90° apart), which help to achieve circular polarization.

Figure 24 shows the simulated axial ratio at different ϕ as a function of θ at 24 GHz for each antenna. The results show that an axial ratio ≤ 3 dB is achieved by each antenna for $\phi=0^\circ$ and $\phi=180^\circ$. Furthermore, the axial ratio is found to improve as the number of elements increases.



(a)



(b)

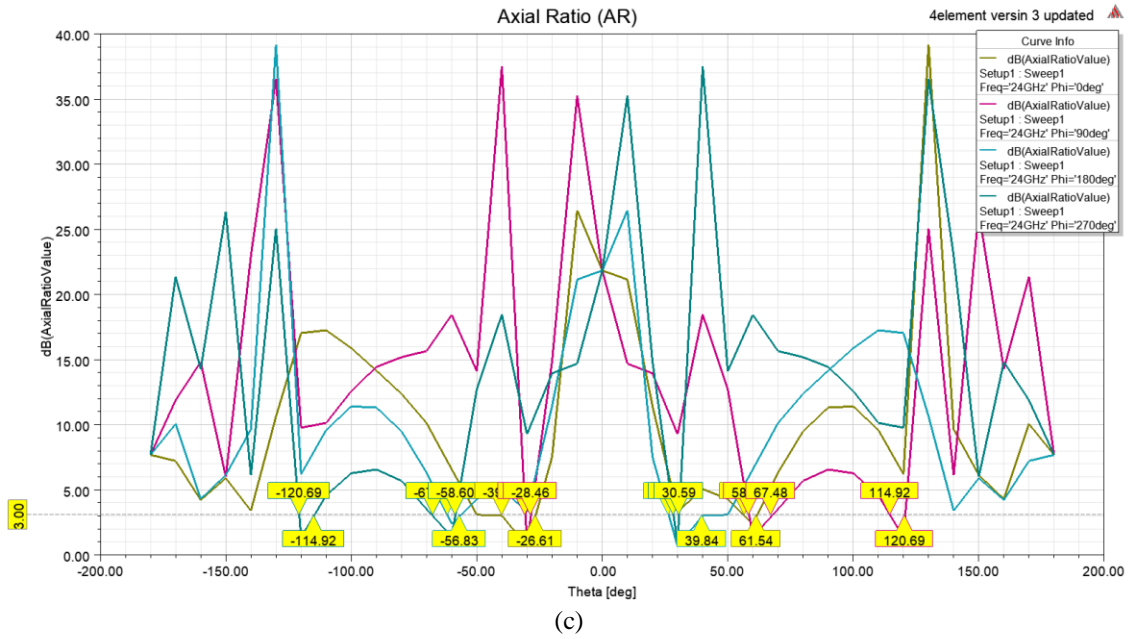


Figure 24: Axial ratio vs Theta (θ) for (a) single-element unit cell; (b) two-element array; (c) four-element array

5.2 Measured Antenna Performance

This section presents the measured return loss $|S_{11}|$ and gain performances of the fabricated antennas. Each antenna is interfaced with the coaxial cable of the VNA using a SMA connector with a specified maximum operating frequency of 26.5 GHz. For the gain measurement, a horn antenna with an operating frequency range between 18–26.5 GHz and a specified gain of 15 dBi is used as the reference antenna. Both the reference and test antennas are positioned approximately 1 m apart. Figure 25 shows an example of measuring the return loss of the unit cell using the VNA.

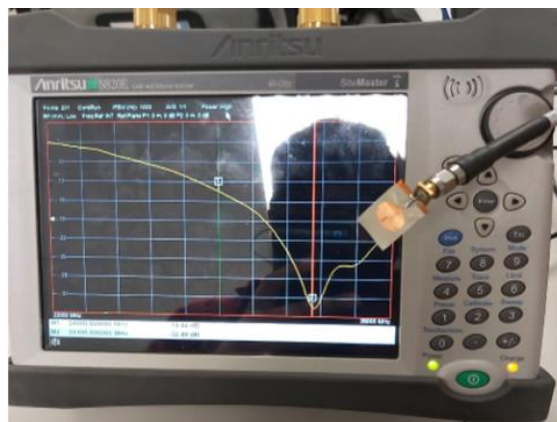
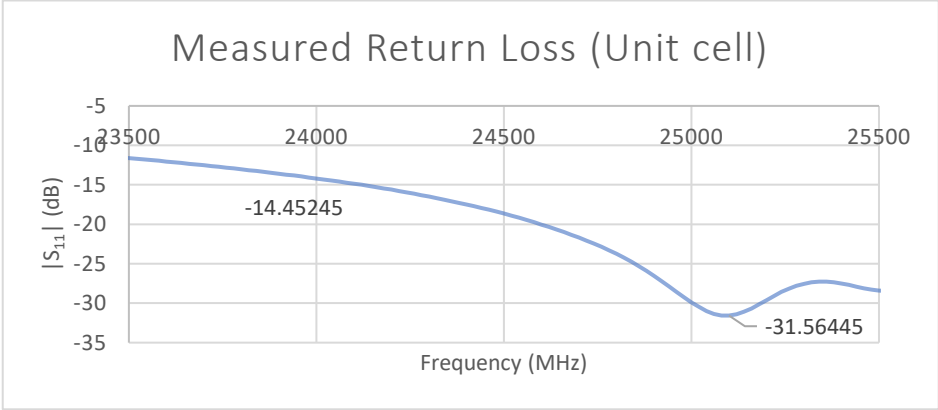
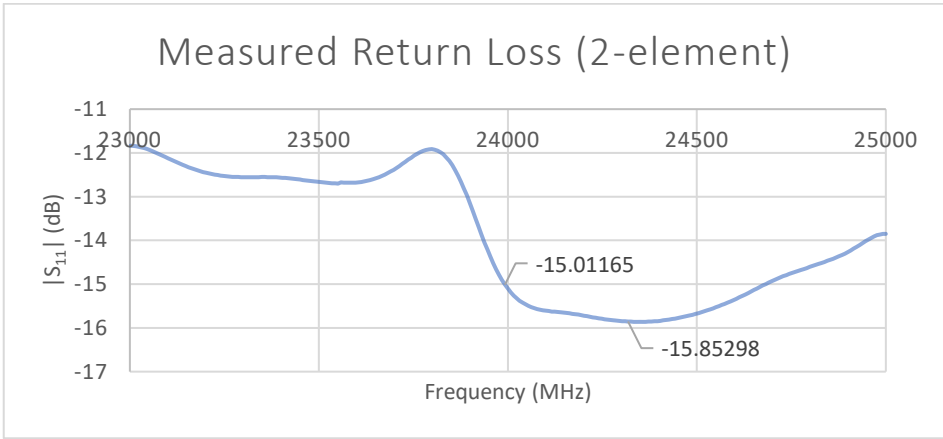


Figure 25: Example return loss measurement of a unit cell using the VNA

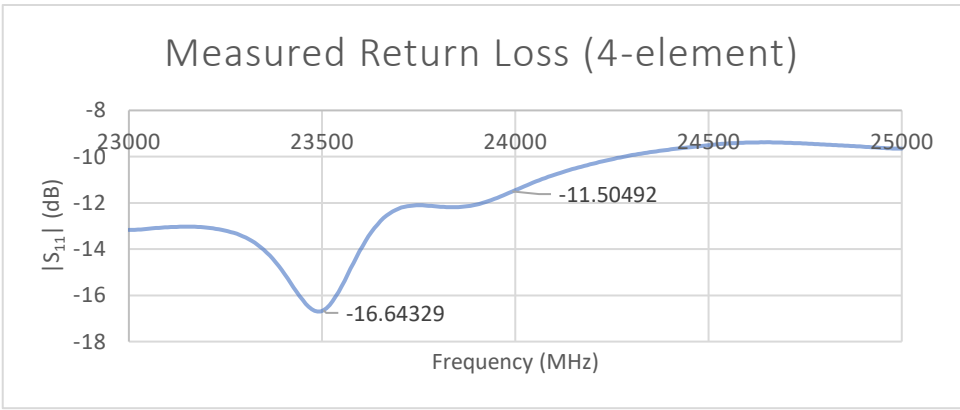
The measured return loss of the unit cell, two- and four-element array are shown in Figure 26. There are apparent differences between the measured and simulated return loss, which may be attributed to fabrication imperfections such as connector soldering. However, the measured return loss at 24 GHz are still better than the minimum requirement of -10 dB for all three fabricated antennas.



(a)



(b)



(c)

Figure 26: Measured return loss of (a) unit cell; (b) two-element array; (c) four-element array

The gain of each fabricated antenna is measured using the gain transfer method (Hillbun 2010) and a 15 dBi horn operating between 18–26.5 GHz as the reference antenna. The measurement steps involve: (i) calibrate the VNA; (ii) measure the S_{21} between the reference and antenna-under-test (AUT); the S_{21} represents the ratio of the received to transmitted power of the antennas as measured by the two ports of VNA; (iii) calculate the path loss between the reference and AUT using the Friis formula $P_L^{dB} = 20 \log_{10} \frac{\lambda}{4\pi d}$ where λ is the signal wavelength (12.5 mm at 24 GHz) and d is the distance between reference and AUT (1000 mm); (iv) obtain the AUT gain as $G_{AUT}^{dB} = S_{21}^{dB} - P_L^{dB} - G_{REF}^{dB}$. Figure 27 shows an example of measuring the S_{21} of the unit cell using the VNA.

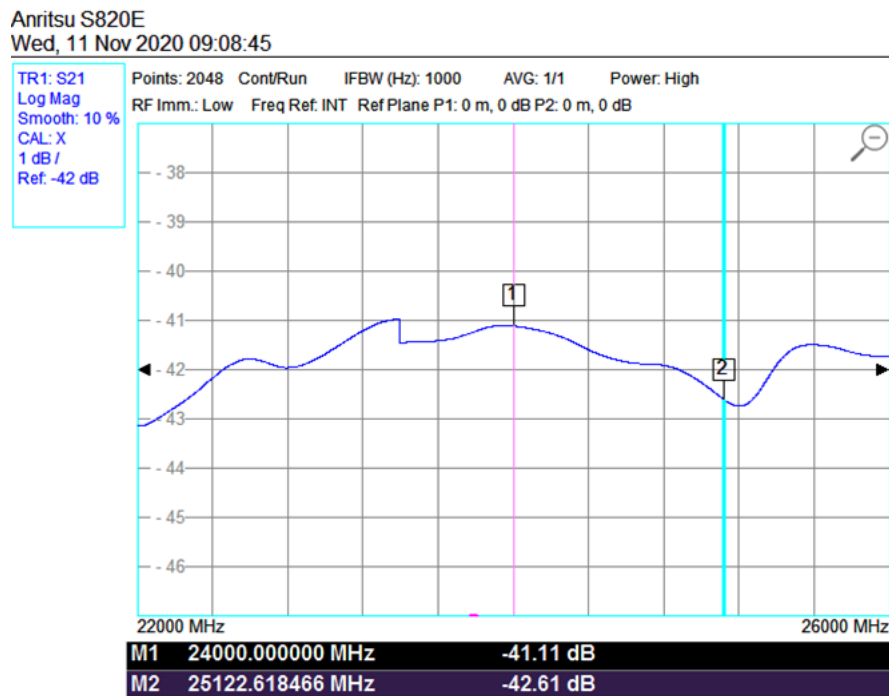
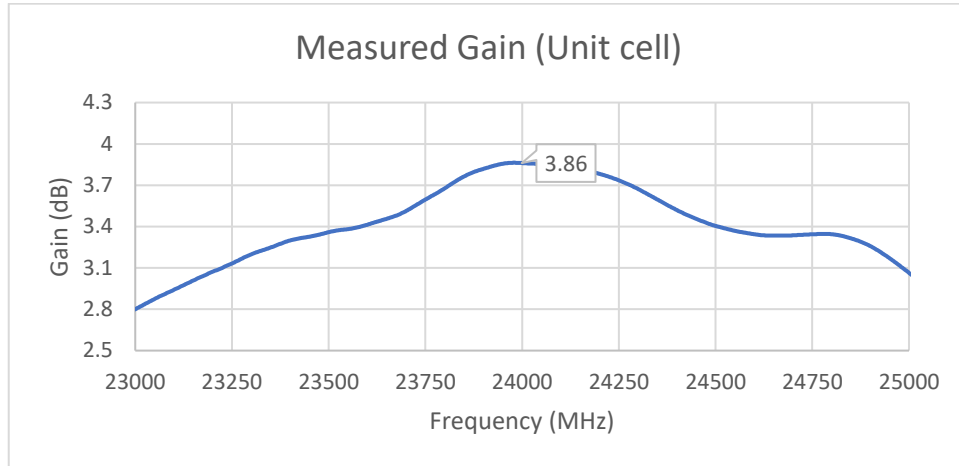
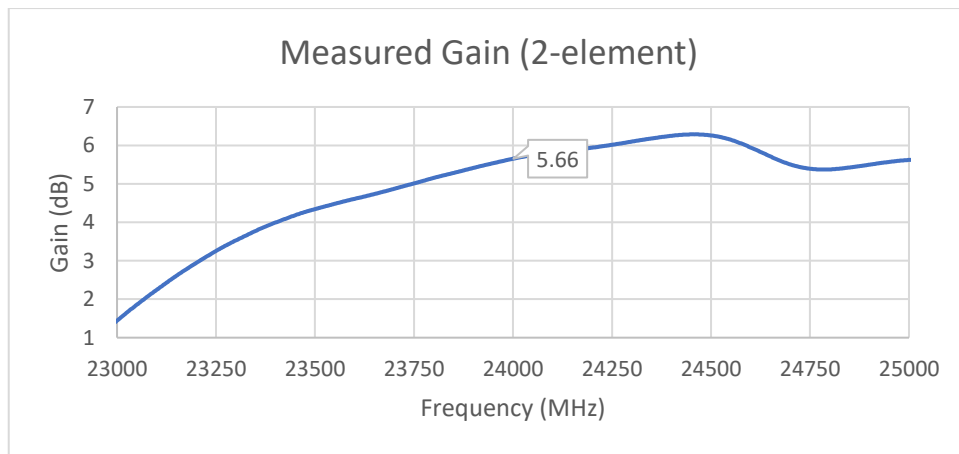


Figure 27: Example S_{21} measurement of a unit cell using the VNA

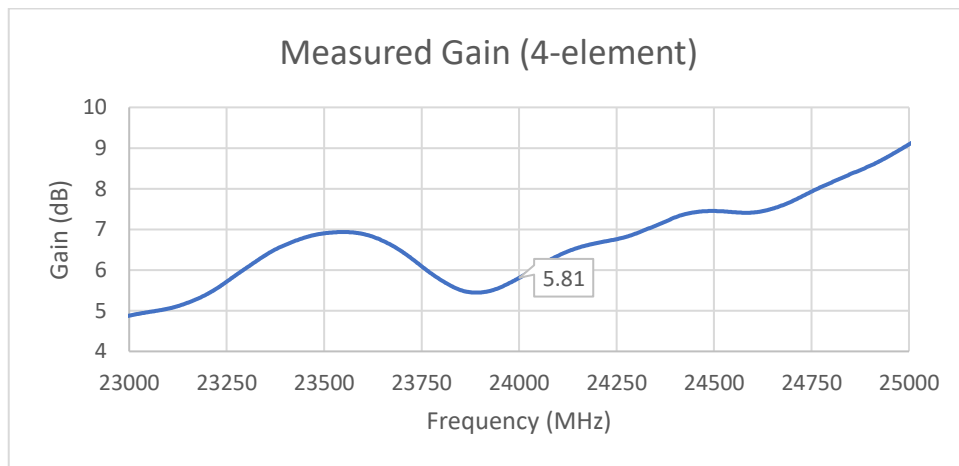
The measured gain of the unit cell, two-, and four-element array are shown in Figure 28. It can be observed that the maximum gain of the unit cell is achieved at a frequency very close to the desired operating frequency of 24 GHz, while those of the two- and four-element arrays occurred at higher frequencies. However, the measured gains of all three antennas at 24 GHz are still significant: 3.86 dBi, 5.66 dBi, and 5.81 dBi, for the unit cell, two-, and four-element array, respectively, which are comparable to the simulated gains shown in Section 6.1.C.



(a)



(b)



(c)

Figure 28: Measured gain of (a) unit cell; (b) two-element array; and (c) four-element array

5.3 Measured Bending Analysis

For analysing the effect of bending on the antenna performance, the fabricated 2-element and 4-element array are positioned on two rolled foams: one with 50 mm, and another with 30 mm diameter. Their return loss $|S_{11}|$ are measured when bended along their horizontal or vertical axis. The 50 mm diameter foam subjects the 2-element and 4-element array to a bending degree of $\sim 65^\circ$, and $\sim 105^\circ$, respectively, while the 30 mm diameter foam subjects each of the same arrays to a bending degree of $\sim 120^\circ$, and $\sim 180^\circ$, respectively.

Figure 29 shows an example setup for a 4-element array bended horizontally on a rolled foam with 50 mm diameter. A comparison of the return loss performance of the 2-element and 4-element array under different bending conditions is shown in Figure 30(a), and 30(b), respectively. It is observed that the bending has not significantly altered their performance. The antennas can still achieve reasonable S_{11} values (< -10 dB) at the desired operating frequency of 24 GHz.

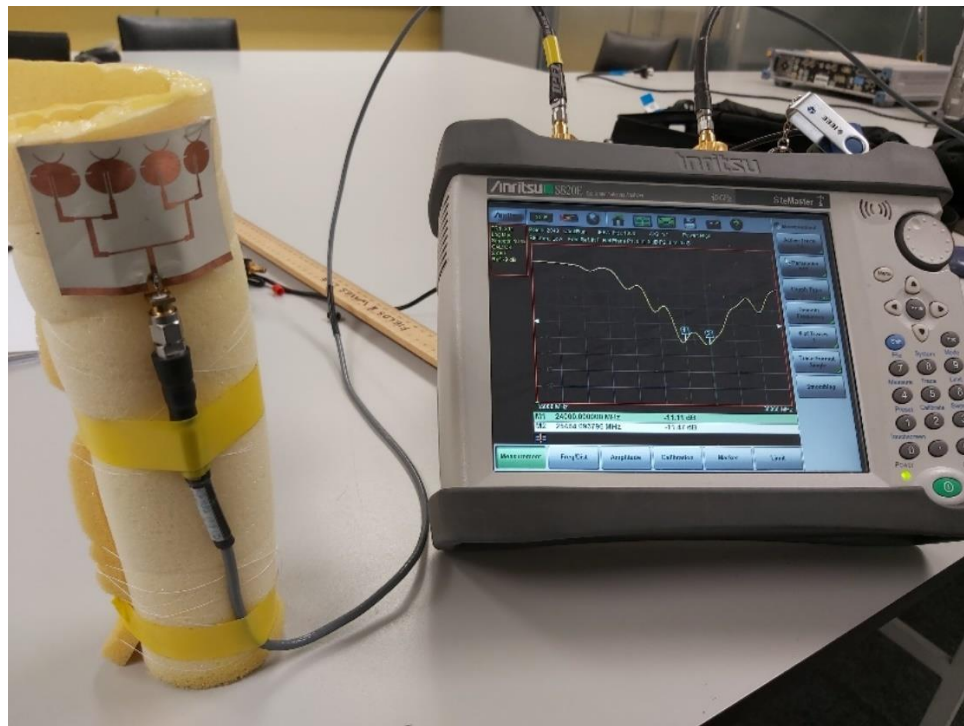


Figure 29: Example measurement setup for bending analysis

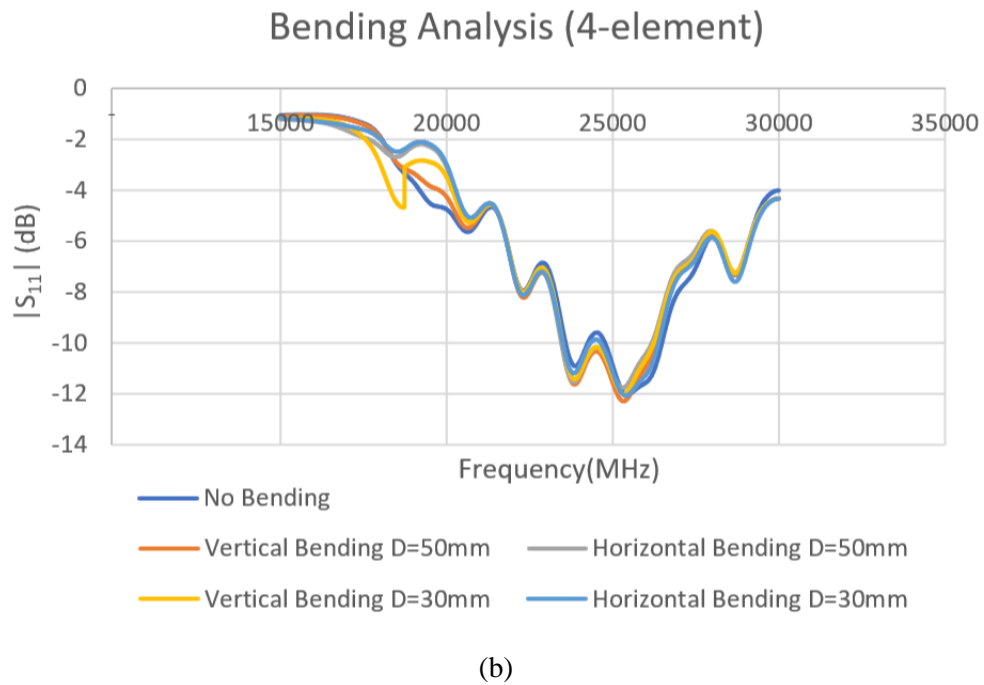
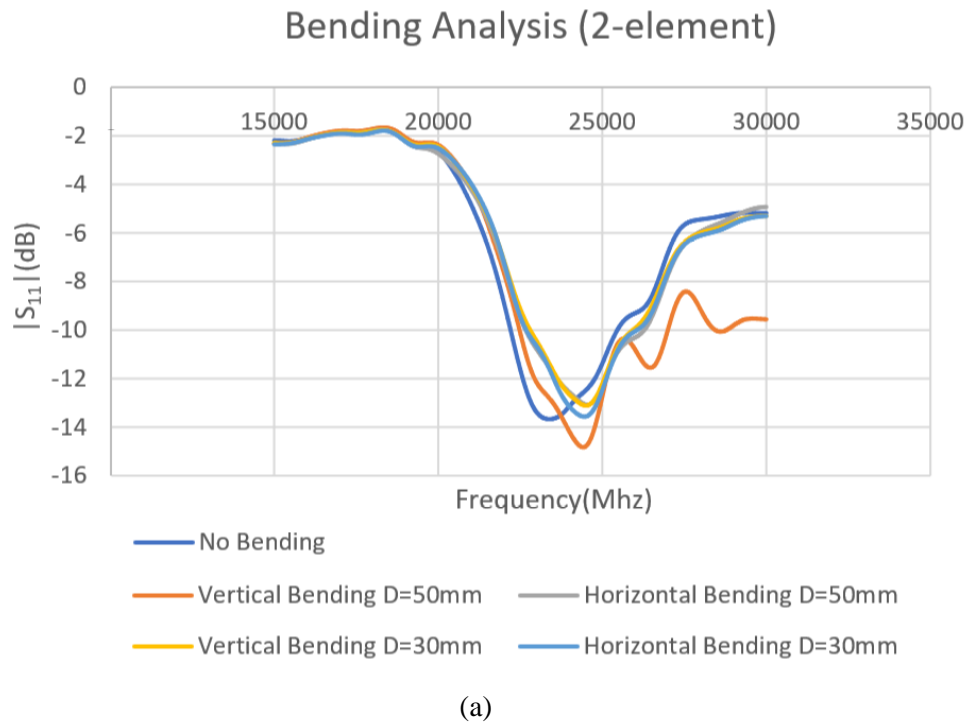


Figure 30: Comparative bending analysis of return loss S_{11} for (a) 2-element array; and (b) 4-element array

5.4 Measured Heart Rate and Breathing Rate

Figure 31 shows an example setup using two 4-element arrays (one for transmit; one for receive) to measure the heart rate (HR) and breathing rate (BR) of a human subject sitting approximately 60 cm from the antennas.

As mentioned in Section 4.4, the setup measures the phase of the S_{21} , which are then processed by a MATLAB program to extract the HR and BR information. The HR/BR of two adult human subjects (one male, one female) are measured. The effectiveness of both two- and four-element arrays are evaluated. For each human subject, the estimated HR/BR are averaged over three measurements (each acquires 2048 signal samples over 18 seconds) and compared with their true values. The true HR is measured by a wrist-worn HR monitor (Figure 32), while the true BR is manually monitored by the subjects by counting the number of breathing cycles during the measurement.

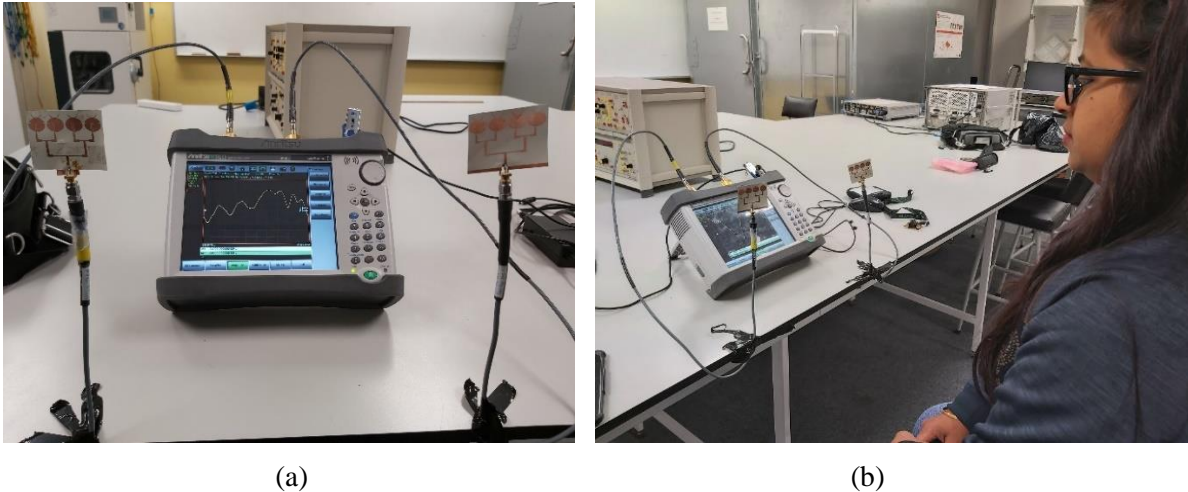


Figure 31: (a) Example setup for HR/BR measurement; (b) Subject sitting in front of the setup



Figure 32: Example measurement of true HR of: (a) Subject 1 (male); and (b) Subject 2 (female); using a wrist-worn HR monitor

Table 2 compares the estimated HR/BR with their true values. One of the human subjects (adult male) clearly has a higher HR than the other, which is correctly detected by our radar system. Generally, the estimated HR/BR are comparable with their true values. However, the percentage error in the estimated BR is observed to be

higher than that in the estimated HR. We believe this is not due to a lower BR detection accuracy, but due to the smaller BR values. For example, with a true BR of 15 and estimated BR of 14, the relative error is 6.67%. But with a true HR of 85 and estimated HR of 84, the relative error is only 1.18% (smaller by more than five times). It is also observed that measurements using the 4-element array give generally more accurate estimations than using the 2-element array.

Table 2: Estimated and True HR and BR from two human subjects

Subject	Antenna Elements	Heart Rate (HR)			Breathing Rate (BR)		
		Estimated	True	Error (%)	Estimated	True	Error (%)
Subject 1	2	97.33	92	5.79	13	15	13.33
Subject 1	4	98	93	5.38	14.33	15	4.47
Subject 2	2	79	76	3.95	16.33	18	9.28
Subject 2	4	81.67	83	1.60	13.67	17	19.59

Figure 33 and 34 shows an example of HR/BR measurement for Subject 1 using two-, and four-element array, respectively. The top figure shows the raw signal of the measured S_{21} phases. The middle figure shows the filtered signal, while the bottom figure shows the signal in frequency domain after FFT. The frequency of the first highest peak identifies the estimated BR, while that of the second highest peak identifies the estimated HR. Figure 35 and 36 shows the equivalent example for Subject 2.

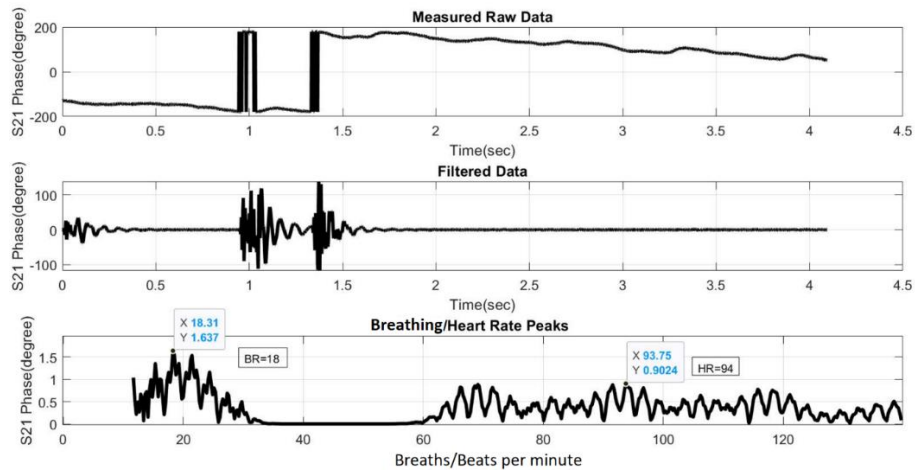


Figure 33: One HR/BR measurement of Subject 1 using two-element array (HR: 94, BR:18)

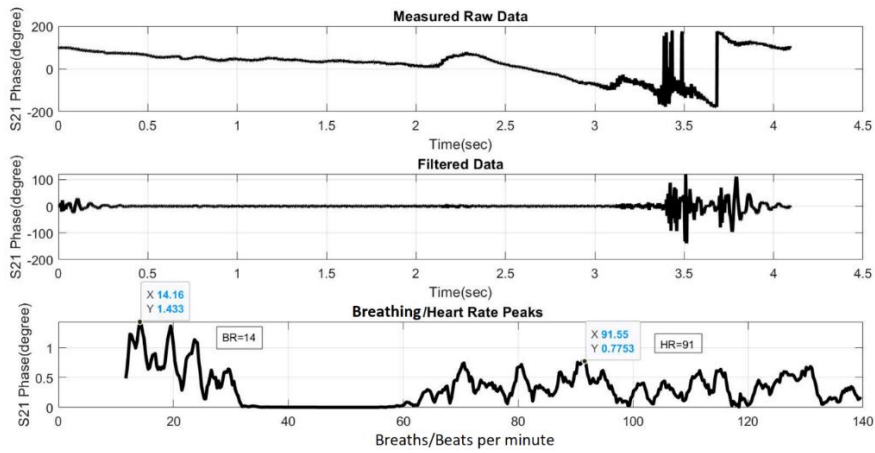


Figure 34: One HR/BR measurement of Subject 1 using four-element array (HR: 91, BR:14)

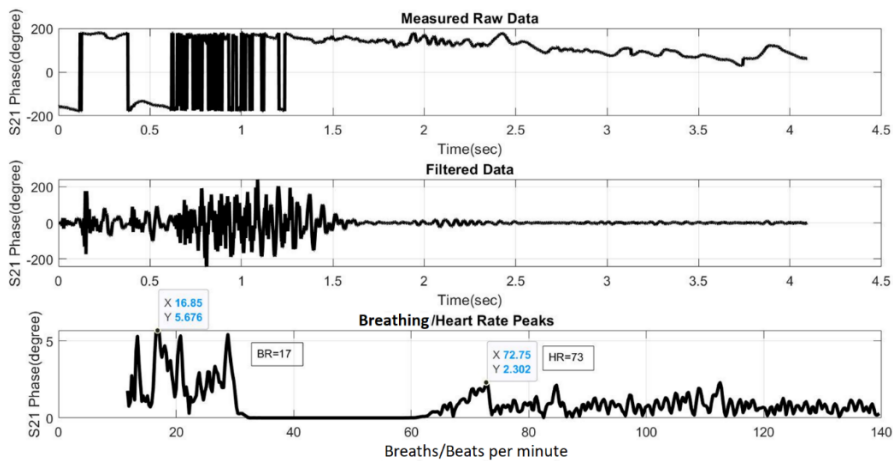


Figure 35: One HR/BR measurement of Subject 2 using two-element array (HR: 73, BR:17)

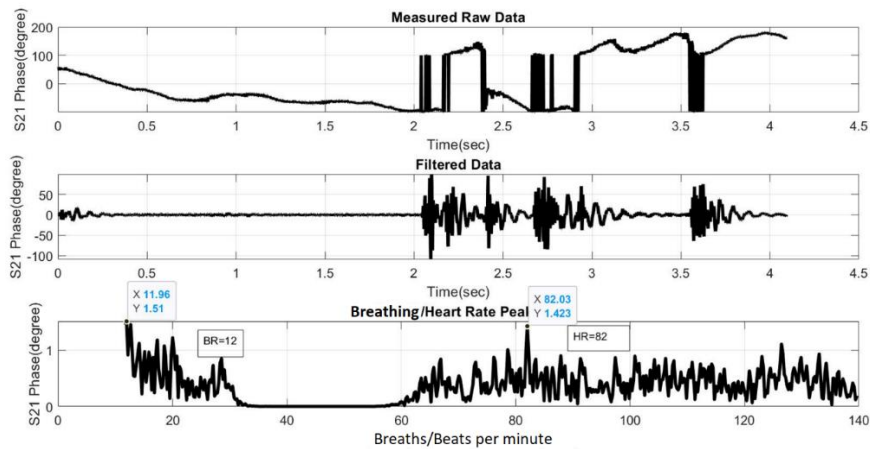


Figure 36: One HR/BR measurement of Subject 2 using four-element array (HR: 82, BR:12)

Chapter 6: Conclusion and Future Work

This thesis firstly presents the design of a single-element unit cell that features an elliptical and horn shaped patch on flexible LCP substrate for 24 GHz bio-radar. The design of two- and four-element arrays using the same unit cell are then presented. The four-element array has the best simulated performance in terms of return loss, gain and axial ratio. It is flexible and thus can conform to the shape of any surface on which it is mounted.

The designed antennas are fabricated, measured, and tested with human subjects to detect their heart and breathing rates. The return loss of all three fabricated antennas are found to exceed the recommended threshold of 10 dB ($|S_{11}| < -10$ dB) at the desired operating frequency of 24 GHz. The estimated heart and breathing rates using the S_{21} information acquired by the fabricated 2- and 4-element arrays from two human subjects are found to be reasonably accurate.

Presently, the detection requires the bio-radar antennas to be positioned in front of a non-moving human subject with an unobstructed view of the chest area. To be feasible for a broader range of applications, the bio-radar should still function well when the human subjects are arbitrarily oriented relative to the antennas, or when they are in arbitrary poses and movements. Hence, some potential directions for future work may include: (i) bio-radar antenna array with steerable beam pattern; (ii) integration of posture and motion detection with vital signs detection; (iii) cooperative vital signs monitoring between bio-radars in a distributed environment; and (iv) low-cost embedded platforms for HR/BR signal acquisition and processing, which are currently performed by expensive VNA and personal computer, respectively.

References

Bailey, R. (2019). "The Cardiac Cycle." Retrieved march 2020, 2020.

Balanis, C. A. (2016). Antenna theory : analysis and design, Wiley.

Bashri, M. S. R., et al. (2015). A dual-band linear phased array antenna for WiFi and LTE mobile applications. 2015 Loughborough Antennas & Propagation Conference (LAPC).

Boothby, A., et al. (2012). Design of Axial-mode Helical Antennas for Doppler-based continuous non-contact vital signs monitoring sensors. 2012 IEEE Radio and Wireless Symposium.

Boric-Lubecke, O., et al. (2015). Doppler Radar Physiological Sensing. New York, UNITED STATES, John Wiley & Sons, Incorporated.

Changzhi, L. and L. Jenshan (2008). Complex signal demodulation and random body movement cancellation techniques for non-contact vital sign detection. 2008 IEEE MTT-S International Microwave Symposium Digest.

D. Obeid (Sept. 2010). Touchless cardiopulmonary monitoring: measurements, processing, and modeling. INSA of Rennes. **Doctoral Thesis**.

Das, V., et al. (2012). Antenna evaluation of a non-contact vital signs sensor for continuous heart and respiration rate monitoring. 2012 IEEE Topical Conference on Biomedical Wireless Technologies, Networks, and Sensing Systems (BioWireless).

Dwivedi, S. (2015). "Comparison and Implementation of Different Types of IIR Filters for Lower Order & Economic Rate." International journal of engineering studies and technical approach, **Volume 01, No. 10, October 2015**.

Fletcher, R. and H. Jing (2009). Low-cost differential front-end for Doppler radar vital sign monitoring. 2009 IEEE MTT-S International Microwave Symposium Digest.

Gouveia, C., et al. (2018). "Bio-radar performance evaluation for different antenna designs." URSI Radio Science Bulletin **2018**(364): 30-38.

Huey-Ru, C., et al. (1991). "Automatic clutter-canceler for microwave life-detection systems." IEEE Transactions on Instrumentation and Measurement, Instrumentation and Measurement, IEEE Transactions on, IEEE Trans. Instrum. Meas. **40**(4): 747-750.

Ian, W. (2018). "Respiratory rate 4: breathing rhythm and chest movement." Nursing Times(114: 9): 49-50.

Iskander, M. F. (1992). Electromagnetic fields and waves, Waveland Press.

Kardo-Sysoev, A. F. (2003). Generation and radiation of UWB-signals. 33rd European Microwave Conference Proceedings (IEEE Cat. No.03EX723C).

Mpanda, R. S., et al. (2018). Investigation on Various Antenna Design Techniques for Vital Signs Monitoring. 2018 Cross Strait Quad-Regional Radio Science and Wireless Technology Conference (CSQRWC).

Mustafa, A. B. and T. Rajendran (2019). "An Effective Design of Wearable Antenna with Double Flexible Substrates and Defected Ground Structure for Healthcare Monitoring System." Journal of Medical Systems **43**(7): 186.

Obeid, D., et al. (2011). Doppler radar for heartbeat rate and heart rate variability extraction: 1-4.

Obeid, D., et al. (2012). "Microwave doppler radar for heartbeat detection vs electrocardiogram." Microwave and Optical Technology Letters **54**(11): 2610-2617.

Rabbani, M. S. and H. Ghafouri-Shiraz (2017). Ultra-Wide Patch Antenna Array Design at 60 GHz Band for Remote Vital Sign Monitoring with Doppler Radar Principle. **38**: 548-566.

Ramachandran, G., et al. (1991). "Reconstruction of out-of-plane cardiac displacement patterns as observed on the chest wall during various phases of ECG by capacitance transducer." IEEE Transactions on Biomedical Engineering **38**(4): 383-385.

Rao, K. R., Yip, P. C. (2001). The transform and data compression handbook. Boca Raton, Fla., CRC Press.

Samad, S. (2017). Contactless detection of cardiopulmonary activity for a person in different scenarios, INSA of Rennes, France and the Lebanese University, Lebanon. **PhD**.

Schäfer, S., et al. (2018). One-dimensional Patch Array for Microwave-based Vital Sign Monitoring of Elderly People. 2018 19th International Radar Symposium (IRS).

Skolnik, M. I. (2008). Radar handbook, McGraw-Hill.

Smith, S. W. (1997). The scientist and engineer's guide to digital signal processing. San Diego, Calif., California Technical Pub.

Srinivasan, D. and M. Gopalakrishnan (2019). "Breast Cancer Detection Using Adaptable Textile Antenna Design." J. Med. Syst. **43**(6): 1-10.

Tan, Y. K. and P. R. P. Hoole (1998). Chirp-signal based processor for radar antennas. IEEE Antennas and Propagation Society International Symposium. 1998 Digest. Antennas: Gateways to the Global Network. Held in conjunction with: USNC/URSI National Radio Science Meeting (Cat. No.98CH36).

Appendix: Matlab Code

REMARKS: This Matlab code is adapted from (Rabbani 2018) for processing measured S_{21} phase data in human bio-radar experiments conducted with a signal frequency of 24 GHz.

```
clear all;
c=3*10^8;
f0=24*10^9;           % frequency
L0=c/f0;              %wavelength
file1=xlsread('nk_2_4.xlsx'); % measured raw data

% Define the filters's cutoff frequencies based on the expected BR and values (1/min)

fb=12;                % Expected min respiration rate/min
fb2=41;               % Expected max respiration rate/min
fh1=61;               % Expected min heart rate/min
fh2=140;              % Expected max heart rate/min
f1=12;
f2=140;               % (f1 and f2 define the range of total expected frequencies)

%%%%%%%%%%%%%% Time Domain Plot %%%%%%%%%%%%%%%

st =4.096
L=length(file1(1:1:end,1)); % total number of samples
fs= L/st;              % sampling frequency
y1=0:st/L:st-st/L;
y2=file1(1:1:end,1);

figure(1);
subplot(311);
```

```

plot(y1,y2,'-k', 'LineWidth',3);
title('Measured Raw Data', 'FontSize',14);
xlabel('Time(sec)', 'FontSize',14);
ylabel('S21 Phase(degree)', 'FontSize',12);
set(gca,'FontSize',12);
grid on

%% Band Pass Filter %%

NF=fs/2; % Nyquist Frequency
[b1,a1]=butter(10,[f1/NF,f2/NF], 'bandpass');
y2=filter(b1,a1,y2);
H1=freqz(b1,a1,y2);
H1=freqz(b1,a1,floor(NF));
Wn=0:1/(NF-1):1;

%% Band Stop Filter %%

[b2,a2]=butter(10,[30/NF,65/NF], 'stop');
y2=filter(b2,a2,y2);
H2=freqz(b2,a2,floor(NF));
Wn=0:1/(NF-1):1;

figure(1)
subplot(312)
plot(y1,y2,'-k', 'LineWidth',3);
title('Filtered Data', 'FontSize',14);
xlabel('Time(sec)', 'FontSize',12);
ylabel('S21 Phase(degree)', 'FontSize',12);
set(gca,'FontSize',12);
grid on

%% DFFT calculations %%

```

```

f=fs*(0:(L/2))/L;
y=fft(y2);
P2=abs(y/L);
P1=P2
fmax=max(f);
Lf=length(f);
gf=fmax/(Lf-1);           %% Frequency interval (frequency bin)
B1=round(fb/gf);         %% Breathing window start frequency
B2=round(fb2/gf);        %% Breathing window end frequency
H1=round(fh1/gf);        %% Heart window start frequency
H2=round(fh2/gf);        %% Heart window end frequency
W1=round(f1/gf);         %% overall window start frequency
W2=round(f2/gf);         %% overall window end frequency

```

```

%% Breathing Rate calculation %%

```

```

[maxB,indxB]=max(P1(B1:B2,1));
BR=(indxB+B1-2)*gf;
fprintf('\nBreathing Rate =%f/min\n',round(BR));
MeanB=mean(P1);
DPhB=maxB;
fprintf('\n Phase variation with breathing =%f Deg..\n', DPhB);

```

```

%% Heart Rate calculation %%

```

```

[maxH, indxH]= max(P1(H1:H2,1));
HR=(indxH+H1-2)*gf;
fprintf('\nHeart Rate =%f/min\n',round(HR));
meanH=mean(P1);
DPhH=maxH;
fprintf('\n Phase variation with Heart=%f Deg.\n', DPhH);

```

```
figure(1)
subplot(313);
plot(f(1,W1:W2), P1(W1:W2,1), '-k', 'LineWidth', 3)
title( 'Breath/Heart Rate Peaks','FontSize', 14);
xlabel( 'Freq(1/min) or Beats per minute (BPM)', 'FontSize',12);
ylabel( 'S21 Phase(degree)', 'FontSize',12);
set(gca,'FontSize',12);
grid on

%%End
```